Lead Optimization of 2-Phenylindolylglyoxyldipeptide MDM-2/TSPO Dual Inhibitors for the Treatment of Gliomas

Simona Daniele,[‡§] Valeria La Pietra,[†§] Elisabetta Barresi, [‡] Salvatore Di Maro,[¶] Eleonora Da Pozzo [‡] Marco Robello,[‡] Concettina La Motta,[‡] Sandro Cosconati,[¶] Sabrina Taliani,[‡] Luciana Marinelli,*[†] Ettore Novellino, [†] Claudia Martini,[‡] Federico Da Settimo.[‡]*

[†] Department of Pharmacy, University of Naples Federico II, Naples, Italy.

[‡] Department of Pharmacy, University of Pisa, Pisa, Italy

[¶] DiSTABiF, Seconda Università di Napoli, Caserta, Italy.

[§] These Authors contributed equally to this work.

KEYWORDS: MDM-2, p53, rational drug design, molecular docking, glioblastoma

ABSTRACT. In Glioblastoma Multiforme (GBM), Translocator Protein (TSPO) and MDM2/p53 represent two druggable therapeutic targets. We recently reported the first dual binder (**1**, TSPO K_i 438 nM; MDM2/p53 IC_{50} 11.65 nM), possessing a higher anticancer effect in GBM cells with respect to the reference standards Nutlin-3 or PK11195 singularly applied. Herein, through a

Structure-Activity-Relationship study, we developed novel derivatives **2-8** with improved potencies toward both TSPO and MDM2. As a result, **7** effectively reactivated the p53 functionality, inhibited viability of two different human p53 wild-type GBM cells, and impaired the proliferation of glioma cancer stem cells (CSCs), known to be intrinsically more resistant to chemotherapeutic agents, and responsible of GBM recurrence. In addition, **7** sensitized both GBM cells and CSCs to the genotoxic activity of Temozolomide, the standard of care for primary GBM. Finally, we preliminary evaluated the safety of **7** showing that its anti-proliferative effect was directed preferentially toward tumour cells with respect to healthy ones. Thus, **7** may represent a promising cytotoxic agent which is worthy to be further developed for a therapeutic approach against GBM, where the downstream p53 signalling is intact and TSPO is over-expressed.

Introduction. Gliomas are the most common primary malignant brain tumors in adults. They can occur anywhere in the central nervous system (CNS), but mostly are intracranial and arise in the glial tissue.[1] Glioblastoma multiforme (GBM), which represents alone the 45% of all gliomas, has been defined by The World Health Organization as a grade IV cancer characterized as malignant, mitotically active, and predisposed to necrosis. Among all gliomas, GBM has the poorest overall prognosis, with only ~5% of patients surviving 5 years past diagnosis.[2] Tumor surgical resection, radiotherapy, and chemotherapy strategies currently used to treat GBM have slowly evolved, and did not lead to significant increases in patient survival. The current standard of care for primary GBM is temozolomide (TMZ), a brain-penetrant alkylating agent that methylates purines (A or G) in DNA and induces apoptosis.[3] However, with TMZ use, risks arise from drug-dependent DNA damage in healthy cells, which becomes heavier considering the possible inefficacy on GBM cells themselves. Along these lines, antiangiogenic therapy for solid tumors, including GBM, has been in the spotlight for many years, and culminated in the development of bevacizumab (Avastin®), a recombinant humanized monoclonal antibody against VEGF-A. Disappointingly, recent data show that bevacizumab, in combination with the standard treatment, did not significantly improve overall patient survival compared to standard treatment alone,[4] while patients experienced a certain impact in terms of angiogenic side effects. It seems that Avastin is more a means to contain GBM growth, rather than to eliminate the tumor.[5]

In addition, GBM has an unfavorable prognosis mainly due to its high propensity for tumor recurrence, the causes of which are complex, and include the high proliferative index of the tumor cells and their resistance to chemotherapy and radiotherapy, particularly in the case of the cancer stem cells (CSCs). It has been proposed that these cells not only initiate the genesis of GBM and contribute to its highly proliferative nature, but are also the basis for its recurrence following treatment. It has also been reported that the most aggressive or refractory cancers contain the highest number of CSCs.[6-8]

Today, it is well known that one of the major causes for treatment failure is the acquired capability of cancer cells to escape apoptosis. In this respect, pharmacological induction of Mitochondrial Outer Membrane Permeabilization (MOMP) through apoptosis inducers[9-11]has emerged as a novel and promising therapeutic approach in a large number of tumors and particularly in GBM.[12] A number of proteins all directly or indirectly regulating the MOMP can be targeted including: (i) p53 tumour suppressor protein, negatively regulated by murine double minute (MDM)-2 and MDM-4, which can induce MOMP by direct interactions with multidomain proteins from the Bcl-2 family; (ii) peculiar components/modulators of the mitochondrial permeability transition pore (MPTP), such as voltage-dependent anion channel (VDAC)[13] or the 18 kDa Translocator Protein (TSPO).[14,15] Along these lines, TSPO ligands, such as Ro5-4864, PK11195, and diazepam, have demonstrated *in vitro* and *in vivo* antitumor properties, both as single agents or combined with etoposide or ifosfamide.[10,16] Noteworthy, in many cellular or animal models, PK11195 (Chart 1) has demonstrated to reduce or abolish the antiapoptotic effect of Bcl-2-family proteins, suggesting that TSPO may be used to bypass Bcl-2-imposed chemoresistance.[17] In this respect, we have demonstrated that newly synthesized selective TSPO ligands are able to induce apoptosis in human GBM cell lines and in rat C6 glioma cells, modulating the opening of the MPT.[18-20]

Very recently, being confident that co-targeting TSPO and MDM2/p53 with one molecule would enhance the antitumor efficacy, we rationally designed and synthesized the first dual binder (compound **1**, Chart 1).[21] This molecule, a 2-phenylindolylglyoxyldipeptide, binding TSPO (K_i 438 nM) and disrupting MDM2/p53 interaction (IC_{50} 11.65 nM), caused MPTP opening, and transmembrane mitochondrial potential ($\Delta\psi m$) dissipation, which in turn resulted in cell-cycle arrest, apoptosis and thus in an anti-proliferative effect on human GBM cells.[21] Interestingly, compound **1** caused both early and late apoptosis death of GBM cells, differently from what observed with the standard MDM2 inhibitor Nutlin-3 (Chart 1), and induced an higher $\Delta\psi m$

collapse with respect to that produced by Nutlin-3 or PK11195 alone.[21] Along these lines, the percentage of GBM cell death was significantly higher with respect to Nutlin-3 and PK11195 singularly applied, suggesting that the simultaneous targeting of MDM2 and TSPO could be useful in blocking tumor cell proliferation.

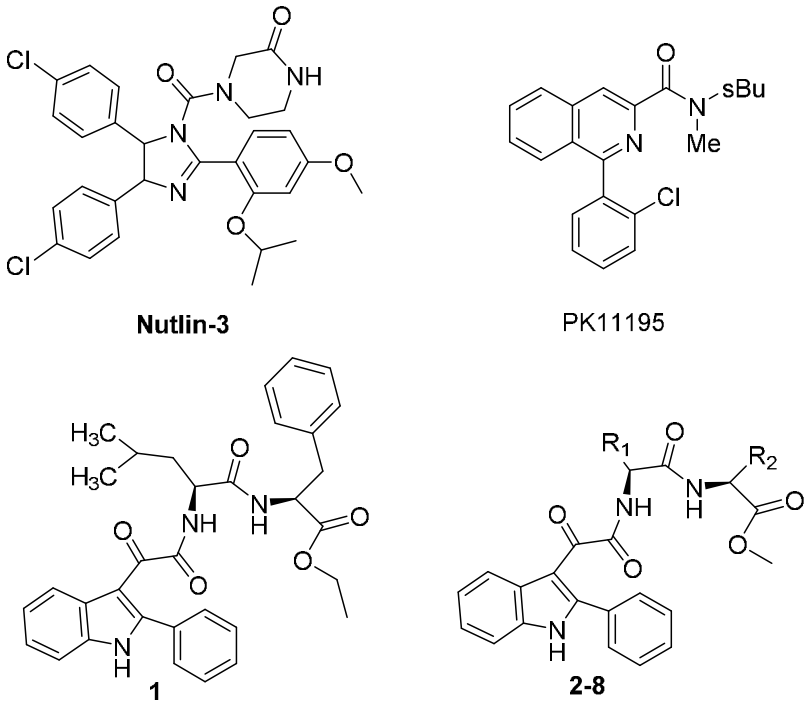

Chart 1.Structures of Nutlin-3, PK11195, known **1**[21] and newly synthesized (**2-8**) 2-phenylindolyl-glyoxyldipeptides.

Herein, through a Structure-Activity-Relationship (SAR) study, we designed and synthesized a novel small library of 2-phenylindolylglyoxyldipeptides **2-8** (Chart 1), featuring different dipeptide moieties on the glyoxylyl bridge. All the new derivatives **2-8** were tested for their ability to bind TSPO and dissociate the MDM2/p53 complex. The best performing compound **7** was then assayed for its ability to reactivate the p53 functionality and to inhibit proliferation/viability of different human GBM cells, as well as of CSCs, a subset of cells within the tumor intrinsically more resistant to chemotherapeutic agents, and responsible of GBM recurrence.[22,23] In addition, as the co-administration of drugs that have different individual targets, but common biological effects, can be

a useful tool in the treatment of cancer, the effects elicited by the co-treatment of GBM cells with compound **7** and TMZ was studied to investigate a potential sinergy of action. Finally, cell viability assays were performed on non-tumoural human Mesenchymal Stem Cells (MSCs), to preliminarily assess the safety of compound **7**.

Results and Discussion

Design and Synthesis. In our previous work,[21] an unsubstituted 2-phenylindolyglyoxylamide (PIGA) was docked in the MDM-2 pocket giving rise to a three-dimensional complex. Subsequently, crystallographic data about p53 helix and MDM2 inhibitors, and the recent knowledge that MDM-2 *N*-terminus region can establish van der Waals and hydrogen bond interactions with small ligands,[24] both suggested how to decorate the PIGA scaffold to target MDM-2 pocket. Thus, similarly to p53 transactivation domain helix, we functionalized the glyoxylylamide group with a Leu residue, and elongated our scaffold in the attempt to reach the region nearby the MDM2 *N*-terminus, by adding a Phe residue. The design strategy resulted in compound **1** (Chart 1), possessing an IC_{50} value of 11.65 nM.[21] As proof of concept of the design hypothesis, docking calculation of **1** in the MDM2 binding site was attempted, and resulted in two main binding poses, where the terminal Phe residue was accommodated within the MDM-2 *N*-terminus region forming hydrophobic contacts with I19, L54, M50 and Y100, and the Leu side chain of **1** occupied the Leu26 pocket, interacting with the Y100, or leaved the Leu26 subpocket unoccupied, getting close to F55 located on the opposite site with respect to the Leu26 pocket (see Figure 1a, hereafter named as "Phe55 pocket").[21]

Noteworthy, our three-dimensional complex showed that in the MDM-2 *N*-terminus region, as well as in the Leu 26 or the Phe55 pocket, either aromatic or aliphatic residues were present. Thus, with the aim of improving the MDM-2 IC_{50}, we thought to convert the terminal phenyl of the lead **1** into aliphatic side chains of different length and/or shape, and the Leu side chain into a phenyl or other aliphatic chains. Moreover, to also improve the TSPO K_i of **1**, our experimental (SARs) and

theoretical data regarding the interactions of PIGA-containing compounds with TSPO were taken into account for the choice of the possible side chain decoration.[33] Indeed, our previous SAR studies and very recent molecular modeling simulations on PIGA compounds, clearly suggested that, although an *N*,*N*-disubstitution at the amide nitrogen was required for an optimal activity towards TSPO, *N*-monosubstituted glyoxylamides featuring highly steric demanding and flexible aliphatic or aromatic groups at the side chain are able to lead to an optimal occupancy of the TSPO L3/L4 lipophilic pockets of the receptor binding site, endowing ligands with nanomolar affinity.[25-29] As a result, a number of combinations (compounds **2-8**) were designed and synthesized.

The experimental procedure for the synthesis of target compounds **2-8** is outlined in Scheme 1. The commercially available 2-phenylindole **9** was acylated with oxalyl chloride, in anhydrous ethyl ether, at 0 °C, to obtain the corresponding 2-phenylindolylglyoxyl chloride **10**,which was allowed to react with the appropriate dipeptides (L-Valine-L-Isoleucine **11**, L-Isoleucine-L-Valine **12**, L-Isoleucine- L-Isoleucine **13**, L-Leucine-L-Valine **14**, L-Valine-L-Leucine **15**, L-Phenylalanine-L-Leucine **16**, L-Phenylalanine-L-Isoleucine **17**) in their methyl ester form, in the presence of triethylamine, in dry toluene, at room temperature for 20-24 h (TLC analysis). At the end of the reaction, the suspension was filtered, and the collected precipitate was washed with a 5% $NaHCO_3$ aqueous solution to yield products **2-8**.

Scheme 1

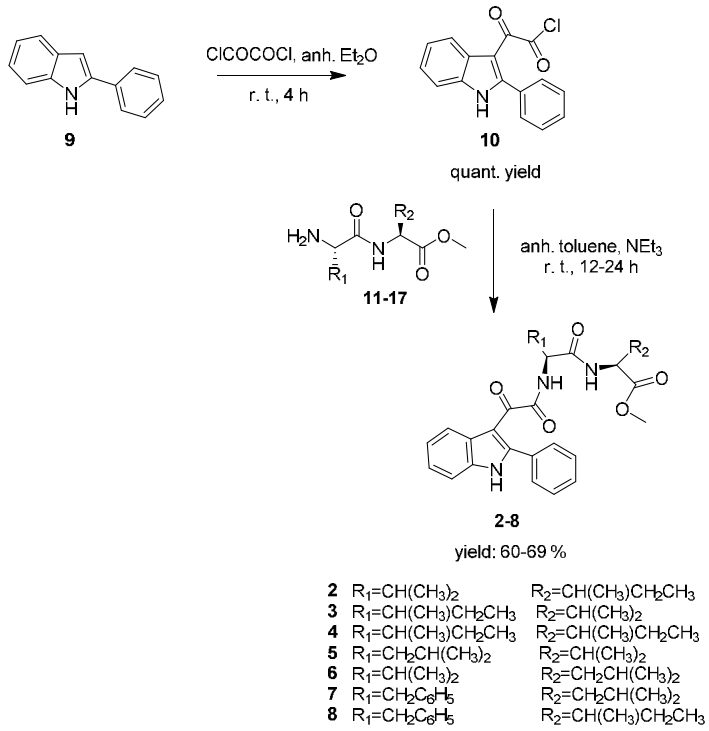

Dipeptides **11-17** were simply obtained in two steps as reported in Scheme 2. Reaction of the appropriate *N*-Boc protected amino acid with the appropriate amino acid methyl ester hydrochloride, in the presence of 1-ethyl-3-(3-dimethylaminopropyl)carbodiimide (EDC) and hydroxybenzotriazole (HOBt) in DMF for 12 hours, yielded derivatives **18-24**. Subsequent deprotection with aqueous trifluoroacetic acid (TFA) furnished the desired dipeptides **11-17**.

Scheme 2

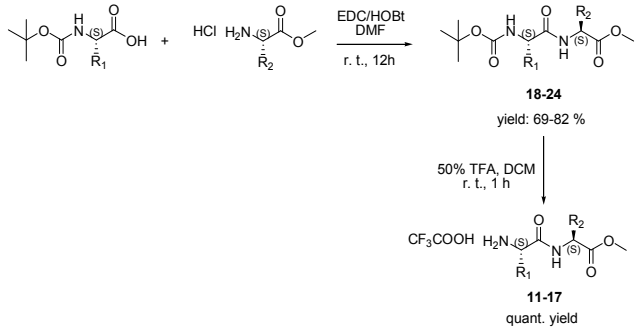

MDM2/p53 complex dissociation and reactivation of p53 function in U87MG cells. The ability of the new compounds to bind MDM2, thus dissociating the MDM2/p53 complex, was investigated

using a quantitative sandwich immune-enzymatic assay technique on native human MDM2/p53 complex. All the tested compounds were able to efficaciously dissociate the MDM2/p53 complex, with IC_{50} values in the nanomolar range (Table 1), and with a potency similar or higher than that of the reference MDM2 inhibitor, Nutlin-3. The dose-response curves for the most potent compounds **2**, **4**, **6**, **7** and **8** are shown in Figure 2. Interestingly, these derivatives showed comparable (**2**, **4**, and **6**) and higher (**7** and **8**) activity with respect to the lead **1** (IC_{50} 11.65 nM), with compound **7** being the best performing one, yielding an IC_{50} value of 4.3 nM.

For this reason, **7** was used in further experiments aimed at confirming the reactivation of p53 pathway, following cell exposure with a MDM2 inhibitor, by assessing accumulation of p53 proteins and induction of p53 target genes.

To these purposes, U87MG cells were used as representative GBM cells. This human cell line resulted an appropriate model to study MDM2-p53 and TSPO pathways, because: i) it maintains a wild type status of p53; ii) it is deficient for the tumour suppressor phosphatase and tensin homologue (PTEN), leading to MDM2 nuclear accumulation, thus inhibiting p53 functions;[30] iii) it expresses high levels of TSPO.[29]

As depicted in Figures 3A and 3B, challenging U87MG cells with 1 μM compound **7** for 8 h led to a significantly increase in p53 protein levels (242 ± 25 % with respect to control cells). Of note, the effect produced by **7** resulted higher with respect to both the parent compound **1** and the reference Nutlin-3. In fact, the lead compound **1** (1 μM) lead to a maximal effect of 173 ± 10 %, while 10 μM nutlin-3 did not significantly affect p53 protein levels at this short time of treatment, in accordance with data previously reported.[21,31] Accordingly, cell treatment with 1 μM **7** led to a significant increase in the mRNA levels of p53 target genes (Figure 4): (i) MDM2, the physiological inhibitor of p53, and its main transcriptional target; (ii) PUMA, a gene required for p53-controlled intrinsic apoptosis pathway; (iii) p21, a cell cycle inhibitor . Specifically, a 3.9-, 4.8- and 5.2-fold of induction of MDM2, PUMA and p21 mRNA, respectively, was observed. These results

demonstrated that stabilization of p53 in **7**-treated cells led to an increase in MDM2, PUMA and p21 mRNA levels in a manner that was consistent with the activation of the p53 pathway. As a comparison, challenging U87MG cells with the lead compound **1** resulted in a 3.3-, 4.1- and 3.9-fold induction of MDM2, PUMA and p21 mRNA, respectively.[21] Overall, these data suggest that **7** is more effective in the reactivation of p53 pathway with respect to both compound **1** and Nutlin-3.

TSPO activity. The compounds exhibiting the highest ability to dissociate the MDM2/p53 complex (i.e., **2**, **4**, **6**, **7** and **8**) were tested for their ability to bind TSPO. For this purpose, radioligand binding assays with the TSPO-selective radioligand [^{3}H]PK11195 were performed. All the tested molecules were able to displace the specific [^{3}H]PK11195 binding, in a concentration-dependent manner (Figure 5), with K_i values in the submicromolar/nanomolar range (Table 2). The highest affinity was displayed by compound **7**, that showed a K_i value about 5-fold lower than that of the lead **1** (**7** K_i 87.2 nM *vs* **1** K_i 438 nM).[21]

Of note, within this class, compound **7** displayed the highest ability to dissociate the p53/MDM2 complex (Table 1), and the highest affinity toward TSPO (Table 2), and both are superior than those of lead **1**.[21] **7** was thus selected for further biological studies.

Molecular Modeling. To explain at molecular level the binding of **7** to both MDM2 and TSPO, molecular modeling studies were attained. In particular, the binding mode of compound **7** was studied by means of docking experiments with the Glide5.5 software in extra precision (XP) mode, using Glidescore for ligand ranking.[32]

As shown in Figure 1, the pose found for **7** in its interaction with MDM2 is very similar to that already described for the lead compound **1**. In particular, the phenyl substituent bound to the indole ring is buried in the Trp23 pocket establishing hydrophobic contacts with L57, I61, F86, F91, I99 and I103 side-chains, while the indole core occupies the MDM2 Phe19 subpocket interacting with I61, M62, V75 and Y67. The glyoxylamide-NH H-bonds with the L54 carbonyl group, while the **7** side chain phenyl ring establishes a π-π interaction with F55. On the other side of the ligand, the

Leu side chain forms hydrophobic contacts with I19, Y100, L54 and M50, while the methyl ester moiety was found close with Q24. Differently from docking results of **1**, pointing out that the ligand Leu side chain can occupy either Leu26 or Phe55 pockets, docking of **7** clearly showed a well-defined binding pose, where the Phe side chain of **7** interacts with F55. This finding would be in line with the lower IC_{50} of **7** and **8** with respect to **1** (12.1 nM for **1** vs 4.3 nM and 9.8 nM for **7** and **8**, respectively) and all other compounds, which do not possess an aromatic R1 substituent (compounds **2**-**6**). Finally, the proposed binding modes of **1** and **7** would explain the higher activity of **4** (IC_{50} 11.7 nM), with respect to the one of **2**, **3**, **5**, and **6** (IC_{50} 15.2 nM, 77.7 nM, 154.6 nM, and 24.8 nM, respectively). Indeed, **4**, by possessing two isoleucine residues, is able to fill up both the Leu26 or Phe55 pockets more efficiently than ligands featuring a valine residue at one of the two residues attached to the PIGA moiety (**2**, **3**, **5** and **6**).

Prompted by our recent theoretical studies on the TSPO receptor, we also attempted at providing a model of the **7**/TSPO interaction starting from a homology-built model of TSPO.[33] As expected, we found for **7** a binding mode that closely resembles the one achieved for other PIGA containing compounds (Figure 6A).[33] In particular, the ligand 2-phenylindole is embedded in a large aromatic cage establishing π-π charge transfer interactions with F20, W53, W95, W107 and W143 residues and hydrophobic contacts with L49, V26, L114. According to this model, the **7** Phe residue directly attached to the PIGA moiety, would place its side chain in the crevice formed by P45 and L31 residues. In the same model, the Leu side chain is embedded in a rather narrow pocket made up by V26, K39, H43, W107 and L150 residues. Indeed, the limited extension of this pocket would explain why docking of **1** resulted in a non well-defined solution. In this respect, manual docking of **1** (Figure 6B) would suggest that the intrinsic rigidity of **1** Phe residue would be hardly adapted in the aforementioned pocket without the concurrent loss of the other key interactions, thus explaining why **7** has a higher affinity for the TSPO receptor than **1**. Similar results (data not shown) were also achieved for **8**, where substitution of the ligand Leu residue with the Ile one would cause a steric

clash between the latter residue $C\gamma^2$ atom and TSPO K39. This would explain why **8** (K_i 504 ± 30 nM) is a weaker TSPO binder when compared with **7** (K_i 87.2 ± 6.8 nM).

Cell apoptosis and cell cycle. The effects of **7** on cellular apoptosis and cell cycle were analysed. Incubation of U87MG cells with **7** (1 μM) for 24 h significantly induced phosphatidylserine externalization, both in the absence (early apoptosis), or in the presence of 7-amino-actinomysin binding to DNA (late apoptosis/death) (Figures 7A and 7B). The total percentage of apoptotic U87MG cells was of 73.7 ± 7.0 (Figures 7A and 7B), whereas 1 μM compound **1** induced a percentage of cell death of 49.0 ± 3.5. Of note, Nutlin-3 did not significantly induce apoptosis at this short time of treatment.[31] These data are consistent with the observed increase of PUMA mRNA level (Figure 4).

Moreover, cell cycle analysis by DNA content analysis revealed an increase in the G2/M fraction after 24h treatment with **7** (Figures 8A and 8B), similarly to previously reported data for compound **1**.[21] These results demonstrated that both the dual-target derivatives are able to trigger GBM cell apoptosis and to arrest cell-cycle progression in the G2/M-phase.

Antiproliferative Activity. To examine the effects of **7** on GBM cell growth/survival, U87MG cells were incubated with different concentrations of **7**. The results showed that the new compound **7** caused a dose-dependent inhibitory effect on U87MG cell viability (Figure 9A), with pharmacological inhibition (IC_{50} value) of 1.2 ± 0.1 μM. As a comparison, compound **1** and Nutlin-3 showed IC_{50} values of 2.6 ± 0.4 μM and 6.5 ± 0.4 μM, respectively. In contrast, the standard TSPO ligand (PK11195) induced a significant inhibition of cell viability starting from 10 μM, and reached a maximal effect at 100 μM (inhibition at 100 μM, 45.0 ± 4.3 % vs control), in line with literature data obtained in human cell lines.[34]

Similar results were obtained in wild-type p53 U343MG cells (Figure 9B), where **1**, **7** and Nutlin-3 showed IC_{50} values of 2.1 ± 0.3 μM, 1.6 ± 0.3 μM and 12.6 ± 1.0 μM, respectively.

The GBM cell line T98G, which expresses mutant p53 was used as a negative control.[35] Following an analogous protocol, compound **7** induced a modest inhibition of T98G cell growth/survival, showing approximately 60% of viable cells at 10 μM (Figure 9C). Treatment of T98G cells with **1** or Nutlin-3 gave similar results (Figure 9C), thus confirming that ligand-mediated antiproliferative effects required a wild-type p53. Of note, PK11195 induced a maximal percentage of 20.3 ± 2.5 % versus control (Figure 9C).

In addition, preliminary viability experiments were performed to evaluate the anti-proliferative potential of compound **7** on glioma CSCs, a GBM subpopolation that has been demonstrated to be more resistant to chemotherapeutic agents, and involved in GBM recurrence.[8,22,23] As depicted in Figure 10A, after 24 h of incubation, compound **7** significantly decreased CSC proliferation at the highest 100 μM concentration; an enhanced antiproliferative effect was observed after prolonged treatment (seven days), with a 25% and 92% depletion of the CSC population at 1 μM and 100 μM **7**, respectively. In parallel experiments, the lead compound **1** and Nutlin-3 induced a slight but significant inhibition of CSC viability, showing a 65% and 45% of CSC depletion at 100 μM after seven days of treatment, respectively (Figure 10A). PK11195 lacked to reduce CSC growth, suggesting that targeting only TSPO is not sufficient to block CSC proliferation.

As co-administration of drugs, having different individual targets, but a common final biological effect, can represent an useful tool in the treatment of GBM, the effect elicited by the co-treatment of GBM cells with the dual-target **7** and the alkylating agent TMZ was studied to investigate a potential sinergy in the antiproliferative activity. In these experiments, a minimum of 72 h cell incubation was chosen, in accordance with previous reports on TMZ.[36] As depicted in Figure 10B, TMZ alone (50 μM) exhibited a reduction in U87MG cell viability of 55% after 72 h. When the alkylating agent was combined with 100 nM **7**, an almost complete depletion of U87MG cells was observed, thus suggesting a synergic/additive effect on the reduction of U87MG cell viability (Figure 10B). Similar results were observed in U87MG-derived CSCs (Figure 10C), thus

demonstrating that the new compound **7** is able to sensitize GBM cells and CSCs to TMZ. Importantly, co-administered drugs are usually employed in lower concentrations than when singularly applied, thus allowing to obtain the same final effect with reduced side effects.

Globally, these data highlight that **7**, being able to target U87MG and U343MG cells, and the CSC subpopulation, can be regarded as a promising lead compound for the development of novel innovative and efficacious anti-proliferative strategy in GBM. A preliminary *in silico* prediction of blood brain (BB) uptake, through QiKProp module of Maestro package,[37] reveals that **7**, based on its lipophilicity, hydrogen bonding capacity, charge, and molecular weight, would not be subject to passive, diffusional uptake. However, it has to be pointed out that any *in silico* prediction totally neglects uptake mechanisms such as carrier-mediated uptake, receptor-mediated transport, and active efflux, that can greatly affect the BB crossing of a drug. Anyway, if the drug alone is not permeable itself, different approaches are nowadays being exploited to help pharmaceuticals to overcome the BB, such as nanotechnologies,[38] and or the so-called "Trojan horse" technology, in which the drug is coupled to a molecule recognized by a receptor-mediated transport system.[39]

Finally, as the selectivity of antitumour agents against cancer cells over the nonmalignant ones is an important issue to be taken into account, the safety of **7** was preliminary tested by evaluating its effect on the viability of non-tumoural human Mesenchymal Stem Cells (MSCs). To this aim, MSCs or U87MG were incubated with different concentrations (ranging from 100 nM to 10 μM) of compound **7** for 48h, and cell viability was measured using MTS assay. As shown in Figure 11, a slight, but significant, reduction of MSC viability was observed at 10 μM. Noteworthy, the effects of **7** on MSC viability were not strictly concentration-dependent, and, most importantly, the percentages of MSC viability reduction were significantly lower with respect to those observed in U87MG cells. Similar results were obtained with the lead compound **1** (Figure 11), suggesting that antiproliferative effects elicited by these derivatives were directed preferentially toward tumour cells.

Conclusions.

Starting from our recent finding of compound **1**[21] as dual-targeting molecule (TSPO and MDM2/p53) endowed with enhanced antitumor efficacy in GBM cells with respect to the reference standards Nutlin-3 or PK11195 alone, we rationally designed a small library of 2-phenylindolylglyoxyldipeptides (**2-8**), featuring different dipeptide moieties on the glyoxylyl bridge. Basically, our three-dimensional complex of MDM-2/**1** showed that in the MDM-2 *N*-terminus region, in the Leu26 as well as Phe55 pockets, either aromatic or aliphatic residues were present. Thus, we though to convert the terminal phenyl of the lead **1** into aliphatic side chains of different length and/or shape, and the Leu side chain into a phenyl or other aliphatic chains (compounds **2-8**). Subsequent biological single-target in vitro screening identified compound **7** as the best performing in terms of TSPO binding affinity and the MDM2/p53 complex dissociation ability. As a result, **7** effectively reactivated the p53 functionality and inhibited human GBM cell growth in vitro by inducing cell cycle arrest and apoptosis. Of note, this compound resulted ineffective in a GBM cell line expressing mutant p53, whereas it was able to inhibit the viability of glioma cancer stem cells (CSCs), a subpopolation of cells within the tumour intrinsically more resistant to chemotherapeutic agents, and responsible of GBM recurrence.[22,23] Finally, cell viability assays performed on non-tumoural human Mesenchymal Stem Cells (MSCs) showed that the anti-proliferative effect elicited by **7** was preferentially directed toward tumour cells. All these findings confirmed that dual targeting p53 and TSPO is a valuable anticancer strategy and that **7** may represent a promising cytotoxic agent which is worthy to be further developed for a therapeutic approach in the treatment of GBM, where the downstream p53 signalling is intact and TSPO is over-expressed.

Table 1. Effect of 2-phenylindol-3-ylglyoxyldipeptides 1,[21] and 2-8 on the dissociation of human p53/MDM2 complex.

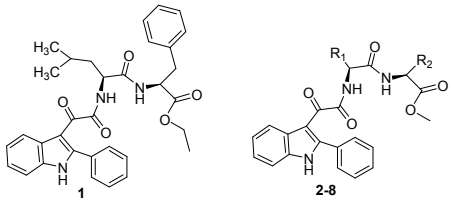

compd	R_1	R_2	IC_{50} (nM)[a]
1[b]	-	-	12.1 ± 0.7
2	$-CH(CH_3)_2$	$-CH(CH_3)CH_2CH_3$	15.2 ± 1.9
3	$-CH(CH_3)CH_2CH_3$	$-CH(CH_3)_2$	77.7± 10.5
4	$-CH(CH_3)CH_2CH_3$	$-CH(CH_3)CH_2CH_3$	11.7 ± 1.2
5	$-CH_2CH(CH_3)_2$	$-CH(CH_3)_2$	154.6 ± 0.8
6	$-CH(CH_3)_2$	$-CH_2CH(CH_3)_2$	24.8 ± 2.7
7	$-CH_2C_6H_5$	$-CH_2CH(CH_3)_2$	4.3 ± 0.6
8	$-CH_2C_6H_5$	$-CH(CH_3)CH_2CH_3$	9.8 ± 0.9
Nutlin-3[b]	-	-	104.5 ± 8.5

[a]Concentration (nM) leading to half-maximal inhibition of p53/MDM2 complex. Data represent the mean values (± SEM) of three independent determinations.

Table 2. Binding Affinity of 2-phenylindol-3-ylglyoxyldipeptides 1,[21] and 2, 4, 6 , 7 and 8 to TSPO. Displacement of specific [^{3}H]PK11195 binding in mitochondrial membranes obtained from rat kidney.

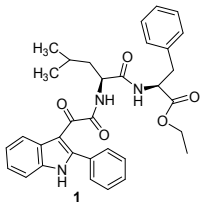

1

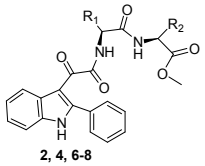

2, 4, 6-8

compd	R_1	R_2	K_i (nM)[a]
1[b]	-	-	430 ± 39
2	-$CH(CH_3)_2$	-$CH(CH_3)CH_2CH_3$	783 ± 60
4	-$CH(CH_3)CH_2CH_3$	-$CH(CH_3)CH_2CH_3$	1004 ± 85
6	-$CH(CH_3)_2$	-$CH_2CH(CH_3)_2$	365 ± 30
7	-$CH_2C_6H_5$	-$CH_2CH(CH_3)_2$	87.2 ± 6.8
8	-$CH_2C_6H_5$	-$CH(CH_3)CH_2CH_3$	504 ± 30
PK11195			3.6 ± 0.5

[a]Data are expressed as means ± SEM derived from a curve-fitting procedure (GraphPad Prism 5).

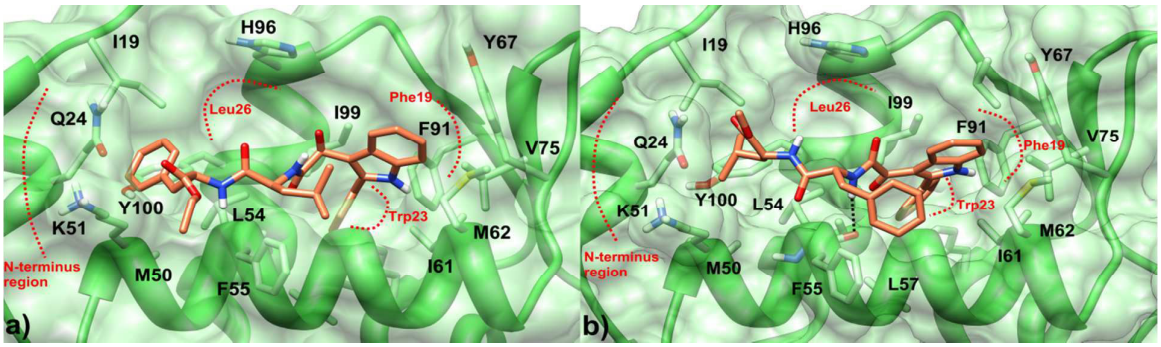

Figure 1. Docking poses of compound **1** (a) and **7** (b) in the MDM2 binding site**.** The ligand is represented as coral sticks, the protein surface as transparent green, and the interacting residues as light green sticks. MDM2 binding pockets are labeled according to p53 interacting side chains and are highlight in red dots.

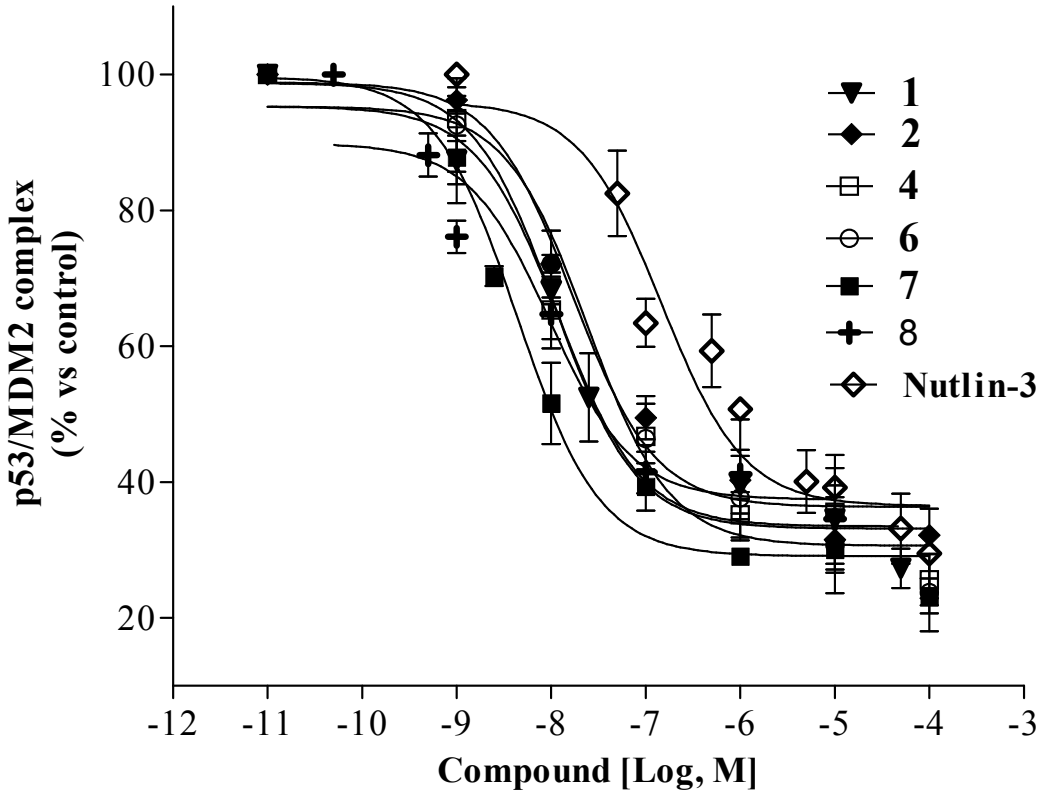

Figure 2. ELISA-based *in vitro* MDM2/p53 protein-protein interaction assay. U87MG cell lysates, containing the native MDM2/p53 complex, were pre-incubated with DMSO (control) or different concentrations of the selected compounds. Then, MDM2 contained in lysate, alone and bound to p53, was captured on MDM2 antibody pre-coated wells. After extensive washes, an antibody specific for p53 was added to the wells and incubated for 90 minutes. The levels of the MDM2/p53 complex were quantified using an HRP-conjugated antibody and a TMB substrate kit. Blank wells were obtained in the absence of p53 antibody. The data were expressed as a percentage with respect to that of untreated cells (control), which was set to 100%, and they are the mean ± SEM of at least three independent experiments. Curves were generated using a sigmoidal dose-response curve model (GraphPad Prism 5 software) from which the IC_{50} values were derived.

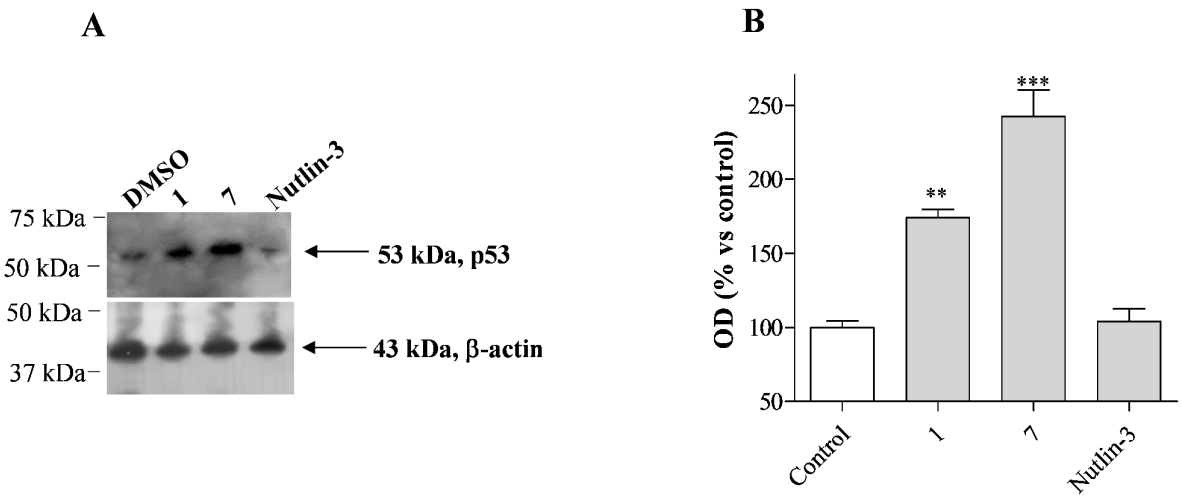

Figure 3. p53 protein accumulation in U87MG cells. The U87MG cells were treated with DMSO (Control), 1 μM **1**, 1 μM **7** or 10 μM Nutlin-3 for 8 h. Lysates were subjected to Western blot analysis using antibody to p53 (FL-393; Santa Cruz Biotechnology). One representative Western blot is presented (panel A) for each cell treatment. β-actin was the loading control. The bar graph (panel B) shows the quantitative analysis of the Western blots, performed using ImageJ. The data were expressed as the percentage of Optical Density (OD) versus control set to 100%, and are the mean ± SEM of three different experiments. Statistical significance was determined with a one-way ANOVA with Bonferroni post-test: **P<0.01, ***P<0.001 vs Control.

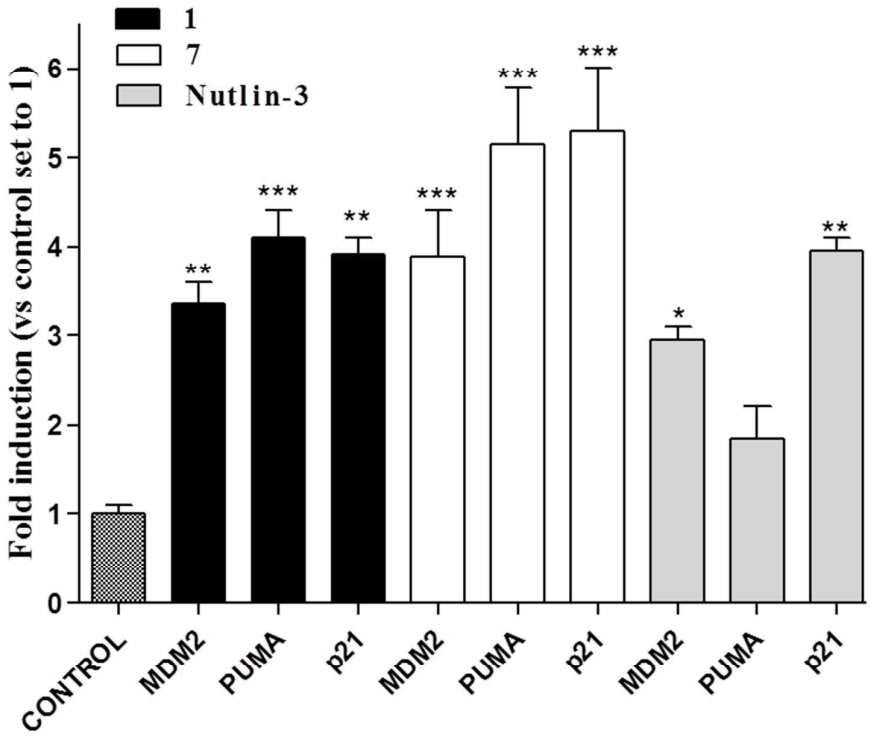

Figure 4. Transcription of p53 target genes in U87MG cells. U87MG cells were treated with DMSO (Control), 1 μM **1**, 1 μM **7** or 10 μM Nutlin-3 for 6 h. The relative mRNA quantification of p53 target genes (PUMA, p21 and MDM2) was performed by real-time RT-PCR as describe in the Methods section. The data were expressed as the fold change versus the levels of the control, and are the mean values ± SEM of three different experiments, each performed in duplicate. The significance of the differences was determined with a one-way ANOVA with Bonferroni post-test: *P<0.05, **P<0.01, *** P<0.001 vs control.

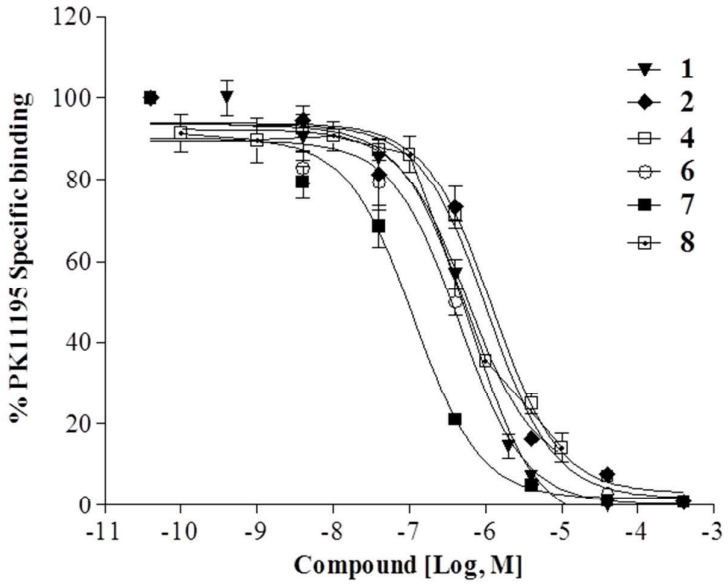

Figure 5. [^{3}H]PK11195 radioligand binding assay. Membranes homogenates obtained from rat kidney (20 µg of proteins) were incubated with 0.6 nM [^{3}H]PK11195 and increasing compound concentrations. Reaching equilibrium, the samples were filtered and bound radioactivity was counted. The data were expressed as percentage of specific binding versus basal value (set to 100%), and are the mean ± SEM of three different experiments. Curves were generated using a sigmoidal dose-response curve model (GraphPad Prism 5 software) from which the IC_{50} values were derived.

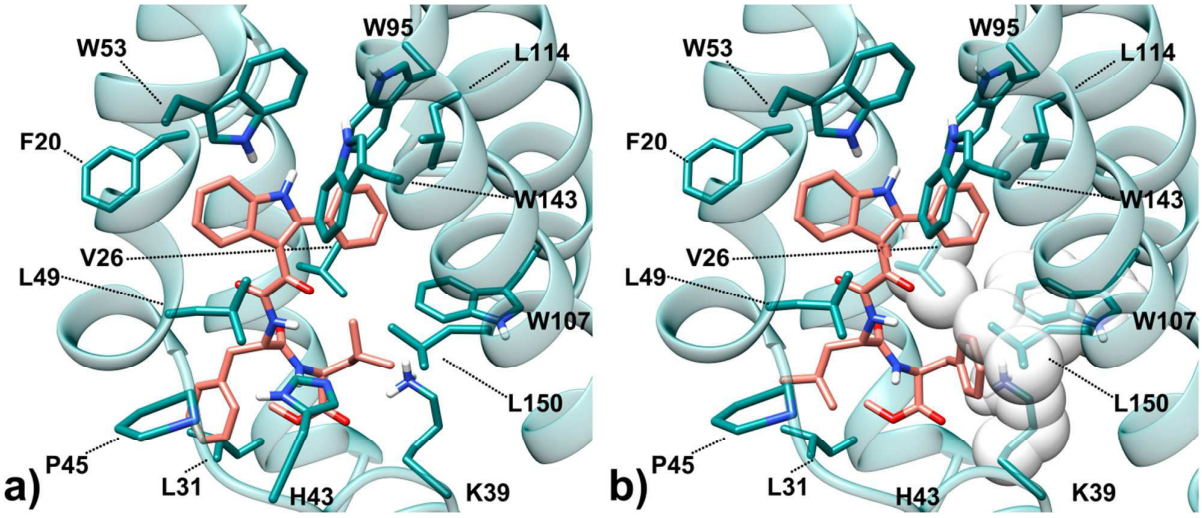

Figure 6. (a) Binding mode of compound **7** in the rat TSPO homology model structure. The ligand is represented as coral sticks while the receptor as cyan sticks and ribbons. (b) Manually docked binding pose of compound **1** in the rat TSPO homology model structure. The ligand is represented as coral sticks while the receptor as cyan sticks and ribbons and white spheres to outline restricted receptor regions.

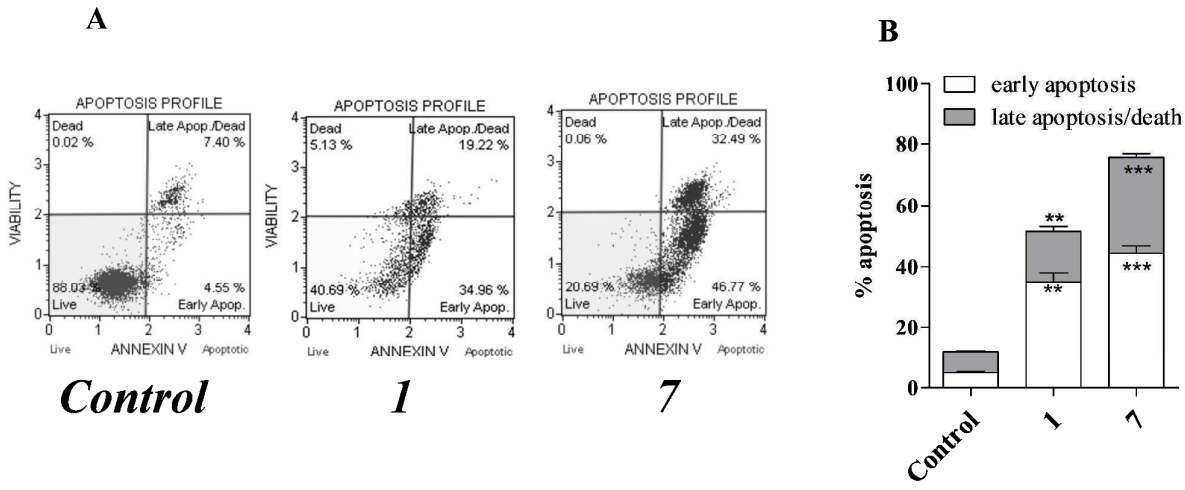

Figure 7. U87MG cell apoptosis. U87MG cells were treated for 24 h with DMSO (control), 1 μM **1** or 1 μM **7**. At the end of the treatment periods, the cells were collected and the level of phosphatidylserine externalisation was evaluated using the Annexin V-staining protocol, as described in the Methods section. b) The data were expressed as the percentage of apoptotic cells (data for the early-stage apoptotic cells shown in white and data for the late-stage apoptotic/necrotic cells shown in grey) versus the total number of cells. The data are the mean ± SEM of three different experiments. The significance of the differences was determined with a one-way ANOVA with Bonferroni post-test: ** P<0.01, *** P<0.001 vs control.

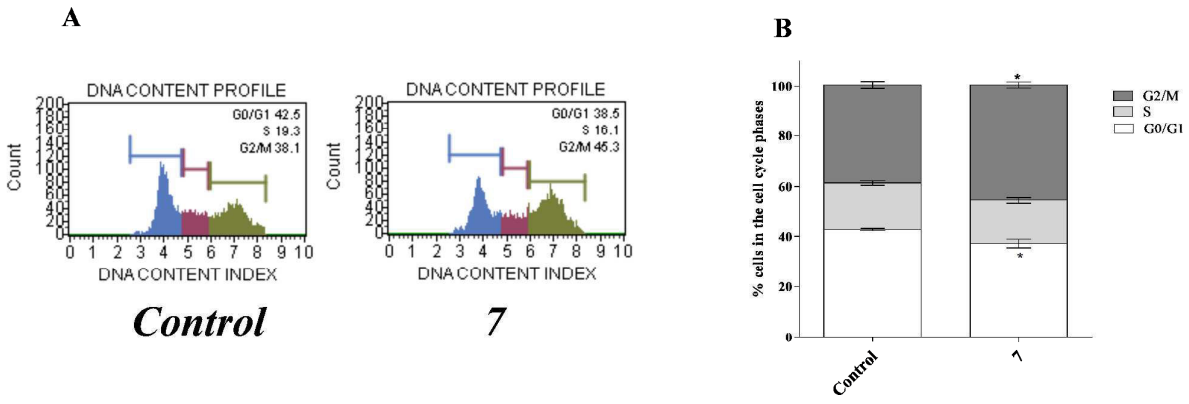

Figure 8. U87MG cell cycle.

U87MG cells were treated for 24h with DMSO (Control), or 1 μM **7**. At the end of the treatment periods, cell cycle was analysed as described in the Methods section. Representative cell cycle histograms of untreated and treated cells were shown (A). The data were expressed as percentage of cell in the different phases (G0/G1, G2 or S) versus total cell number, and they are the mean values ± SEM of three different experiments. The significance of the differences was determined with a one-way ANOVA with Bonferroni post-test: * $P<0.05$ vs control in the respective cellular phase.

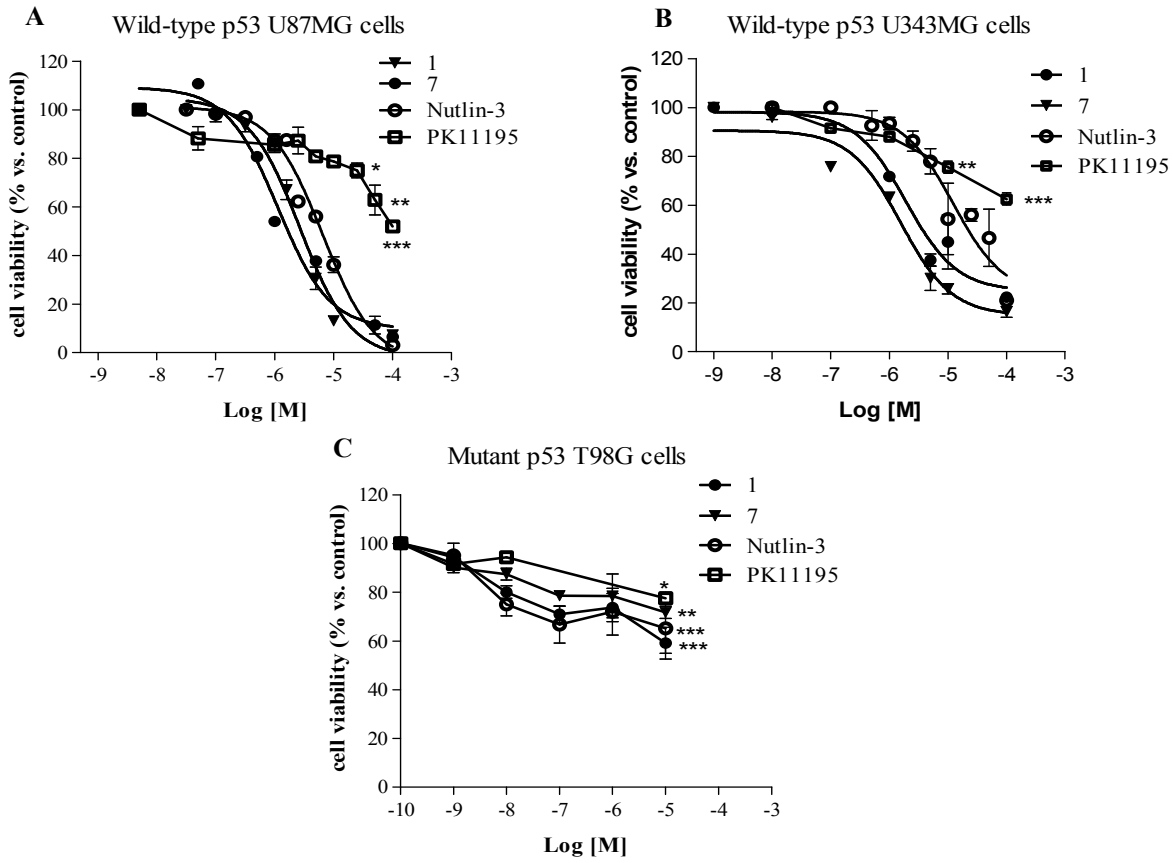

Figure 9. Evaluation of in vitro anti-proliferative effect. U87MG **(A)**, U343MG (**B**) or T98G (**C**) cells were incubated with increasing concentrations of **1**, **7**, Nutlin-3 or PK11195, and cell viability was assessed after 48 h of treatment by MTS assay. The data were expressed as a percentage with respect to that of untreated cells (control), which was set to 100%. Curves were generated using a sigmoidal dose-response curve model (GraphPad Prism 5 software), from which the IC_{50} values were derived. The data were expressed as a percentage with respect to that of untreated cells (control), which was set to 100%, and are the mean values ± SEM of three independent experiments, each performed in duplicate. The significance of the differences was determined with a one-way ANOVA with Bonferroni post-test: * P<0.05, ** P<0.01, *** P<0.001 vs control.

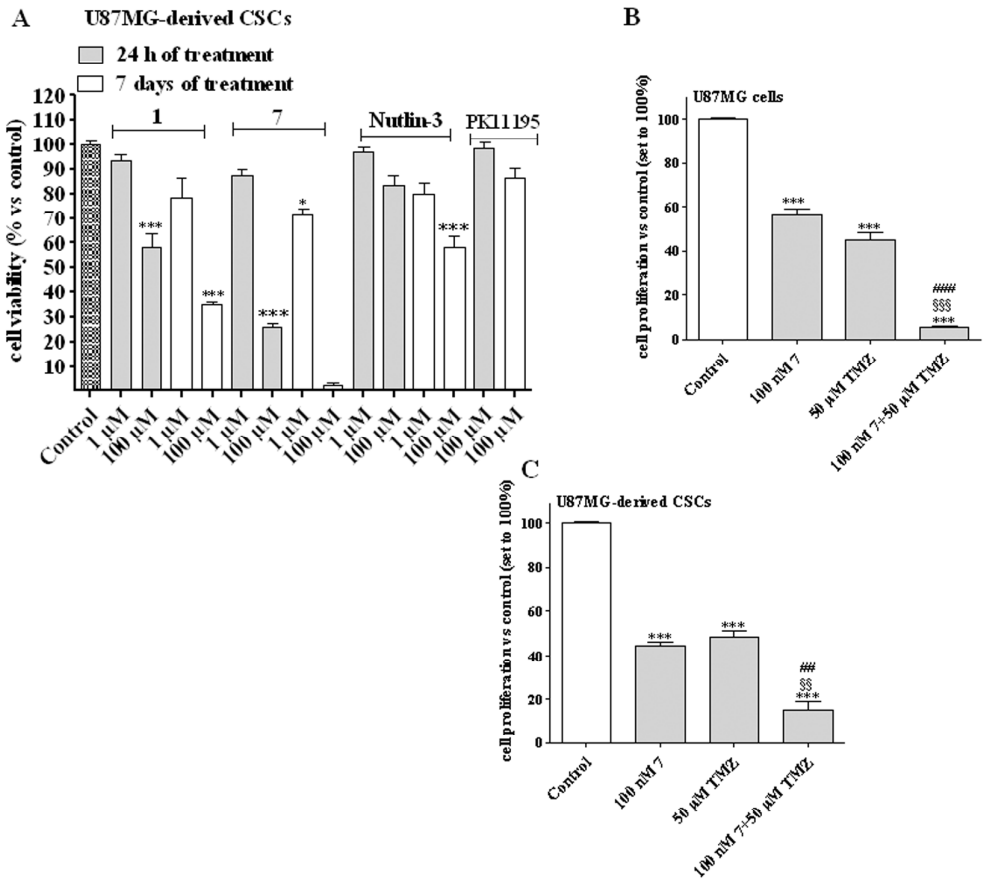

Figure 10. Effects on CSC viability and of TMZ co-treatment. (**A**) CSCs isolated from U87MG cells were incubated with the indicated concentrations of **1**, **7**, Nutlin-3 or PK11195 for 24 h or seven days. At the end of treatment, cell viability was measured using MTS assay. The data were expressed as a percentage with respect to that of untreated cells (control), which was set to 100%, and are the mean values ± SEM of three independent experiments, each performed in duplicate. The significance of the differences was determined with a one-way ANOVA with Bonferroni post-test: * P<0.05, *** P<0.001 vs. control. (B, C) U87MG cells (panel B) or U87MG-derived CSCs (panel C) were incubated with 100 nM **7** or 50 μM TMZ for 72 h or seven days, respectively. At the end of treatment, cell viability was measured using MTS assay. The significance of the differences was determined with a one-way ANOVA with Bonferroni post-test: * P<0.05, *** P<0.001 control; ## P<0.01, ### P<0.001 vs. cells treated with **7**; §§ P<0.01, §§§ P<0.001 vs. cells treated with TMZ.

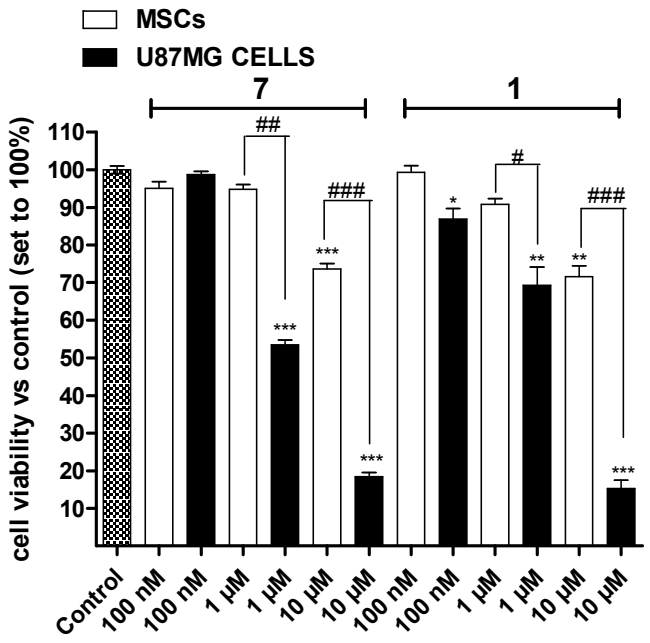

Figure 11. Effects on the viability of normal MSCs. MSCs or U87MG were incubated with the indicated concentration of **1** or **7** for 48 h. At the end of treatment, cell viability was measured using MTS assay. The data were expressed as a percentage with respect to that of untreated cells (control), which was set to 100%, and are the mean values ± SEM of three independent experiments, each performed in duplicate. The significance of the differences was determined with a one-way ANOVA with Bonferroni post-test: * $P<0.05$, ** $P<0.01$, *** $P<0.001$ control; # $P<0.05$, ## $P<0.01$, ### $P<0.001$ vs MSCs.

Experimental Section

Chemistry. Melting points were determined using a Reichert Kofler hot-stage apparatus and are uncorrected. Routine nuclear magnetic resonance spectra were recorded in $CDCl_3$ or DMSO-d_6 solution on a Varian 400 spectrometer operating at 400 MHz or Varian Gemini 200 spectrometer operating at 200 MHz. Evaporation was performed in vacuo (rotary evaporator). Analytical TLC was carried out on Merck 0.2 mm precoated silica gel aluminum sheets (60 F-254). Optical rotatory powers ([α]D) were determined using a Perkin Elmer model 343 polarimeter, at a temperature of 22 °C. All the target products undergoing biological testing were >96% pure as demonstrated by analysis carried out with a Varian Prostar HPLC system equipped with an PDA Detector at 260 nm (column Luna C18 (2) 5µ (150 mm x 4.6 mm)), gradient A/B 80/20 to 20/80 in 20 min, A consisting of water, B consisting of acetonitrile, flow rate of 1 ml/min, room temperature). 2-Phenylindol-3-ylglyoxyl chloride **9** was prepared according with a reported procedure.[25,26]

General procedure for the synthesis of 2-(phenylindol-3-yl)-glyoxyldipeptide derivatives 2-8. Oxalyl chloride (0.31 ml, 3.6 mmol) was added dropwise, at 0 °C to a well-stirred mixture of the commercially available 2-phenylindole **9** (0.580 g, 3.0 mmol) in freshly distilled diethyl ether (10 ml). The mixture was maintained at room temperature for 4 h. The generated precipitate was collected by vacuum filtration to give the glyoxylyl chloride **10** that was directly used in the subsequent reaction. A solution of the appropriate dipeptide in their methyl ester form [H_2N-Val-Ile-OMe **11**; H_2N-Ile-Val-OMe **12**; H_2N-Ile-Ile-OMe **13**; H_2N-Leu-Val-OMe **14**; H_2N-Val-Leu-OMe **15**;H_2N-Phe-Leu-OMe **16;** H2N-Phe-Ile-OMe **17**], (2.0 mmol) in 5 mL of dry toluene was added dropwise to a stirred suspension, cooled at 0°C, of the 2-phenylindol-3-ylglyoxyl chloride **9** (0.567 g, 2.0 mmol), in 15 mL of the same solvent, followed by addition of triethylamine (0.34 mL, 2.4 mmol). The reaction mixture was allowed to warm to room temperature, stirred for 12-24 hours (TLC analysys) and then filtered. The collected precipitate was triturated with a 5% $NaHCO_3$ aqueous solution and collected again to give a first portion of crude product. The toluene solution was removed under reduced pressure, the residue was dissolved with CH_2Cl_2 and the organic

solution was washed with 5% $NaHCO_3$ aqueous solution, H_2O, 10% HCl, and finally H_20. After drying with $MgSO_4$ the dichloromethane was evaporated to dryness to yield an additional amount of crude product. Products **2-8** were finally purified by washing with cold diethyl ether.

*2-(Phenylindol-3-yl)glyoxyl-(L)-Valine-(L)-Isoleucine methyl ester***2.** Yield 66%; mp 92-94 °C; $[\alpha]^{22}_D$ = -27° (c = 2.0 mg/mL in MeOH); ^{1}H NMR (200 MHz, DMSO-d_6, ppm) δ 0.81-0.84 (m, 12H); 1.21-1.43 (m, 2H); 1.76-1.85 (m, 2H); 3.59 (s, 3H); 4.05-4.24 (m, 2H); 7.18-7.28 (m, 3H); 7.41-7.56 (m, 3H); 7.94-7.97 (m, 1H); 8.24 (d, J = 7.0 Hz, 1H); 8.56 (d, J = 8.8 Hz, 1H); 12.36 (bs, 1H). ^{13}C NMR (100 MHz, DMSO-d_6, ppm) δ 11.70, 15.85, 18.77, 19.37, 25.41, 31.36, 36.61, 51.96, 57.06, 57.54, 109.36, 112.42, 121.26, 122.51, 123.63, 127.89, 128.53, 129.63, 129.98, 131.98, 136.28, 147.29, 166.67, 170.99, 172.21, 187.20.

*2-(Phenylindol-3-yl)glyoxyl-(L)-Isoleucine-(L)-Valine methyl ester***3.** Yield 60%; mp 108-110 °C; $[\alpha]^{22}_D$ = -31° (c = 2.0 mg/mL in MeOH); ^{1}H NMR (200 MHz, DMSO-d_6, ppm) δ 0.81-0.94 (m, 14H); 1.41-1.44 (m, 1H); 1.63-1.66 (m, 1H); 3.61 (s, 3H); 4.13-4.20 (m, 2H); 7.14-7.29 (m, 2H); 7.44-7.46 (m, 4H); 7.60-7.64 (m, 2H); 7.94-7.98 (m, 1H); 8.23 (d, J = 7.4 Hz, 1H); 8.58 (d, J = 9.2 Hz, 1H); 12.36 (bs, 1H). ^{13}C NMR (100 MHz, DMSO-d_6, ppm) δ 11.45, 15.42, 18.90, 19.36, 24.84, 30.13, 37.41, 52.00, 56.69, 58.13, 109.33, 112.42, 121.22, 122.48, 123.61, 127.86, 128.55, 129.65, 129.96, 131.98, 136.28, 147.26, 166.57, 171.13, 172.20, 187.14.

*2-(Phenylindol-3-yl)glyoxyl-(L)-Isoleucine-(L)-Isoleucine methyl ester***4.** Yield 63%; mp 98-100 °C; $[\alpha]^{22}_D$ = -30° (c = 2.0 mg/mL in MeOH); ^{1}H NMR (200 MHz, DMSO-d_6, ppm) δ 0.79-0.89 (m, 12H); 1.19-1.21 (m, 3H); 1.74-1.76 (m, 3H); 1.74-1.76 (m, 3H); 3.59 (s, 3H); 4.14-4.19 (m, 2H); 7.16-7.24 (m, 2H); 7.42-7.58 (m, 4H); 7.58-7.62 (m, 2H); 7.93-7.97 (m, 1H); 8.24 (d, J = 7.6 Hz, 1H); 8.56 (d, J = 8.8 Hz, 1H); 12.35 (bs, 1H). ^{13}C NMR (100 MHz, DMSO-d_6, ppm) δ 11.45, 11.70, 15.41, 15.84, 24.85, 25.43, 36.60, 37.47, 51.94, 56.64, 57.06, 109.34, 112.43, 121.22, 122.48, 123.61, 127.87, 128.54, 129.63, 129.97, 131.99, 136.28, 147.26, 166.56, 171.05, 172.16, 187.15.

*2-(Phenylindol-3-yl)glyoxyl-(L)-Leucine-(L)-Valine methyl ester***5.** Yield 67%; mp 101-103 °C; $[\alpha]^{22}_D$ = -34° (c = 2.0 mg/mL in MeOH); ^{1}H NMR (200 MHz, DMSO-d_6, ppm) δ 0.79-0.90 (m,

12H); 1.22-1.34 (m, 4H); 3.59 (s, 1H); 4.12-4.25 (m, 2H); 7.13-7.27 (m, 4H); 7.44-7.48 (m, 3H); 7.56-7.60 (m, 1H); 7.96-7.99 (m, 1H); 8.17 (d, J = 8.2 Hz, 1H); 8.65 (d, J = 8.6 Hz, 1H); 12.30 (bs, 1H). ^{13}C NMR (100 MHz, DMSO-d_6, ppm) δ 18.81, 19.36, 22.63, 23.24, 24.47, 30.29, 41.38, 51.05, 52.09, 57.93, 109.41, 112.42, 121.29, 122.53, 123.66, 127.87, 128.60, 129.72, 129.95, 131.95, 136.28, 147.37, 166.39, 172.06, 172.25, 187.18.

*2-(Phenylindol-3-yl)glyoxyl-(L)-Valine-(L)-Leucine methyl ester***6.** Yield 66%; mp 108-110 °C; $[\alpha]^{22}_D$ = -32° (c = 2.0 mg/mL in MeOH); ^{1}H NMR (200 MHz, DMSO-d_6, ppm) δ 0.82-0.93 (m, 12H); 1.52-1.57 (m, 3H); 1.89-1.96 (m, 1H); 3.59 (s, 3H); 3.90-4.17 (m, 1H); 4.23-4.31 (m, 1H); 7.17-7.25 (m, 2H); 7.40-7.45 (m, 3H); 7.49- 7.63 (m, 2H); 7.95-7.99 (m, 1H); 8.34 (d, J = 7.0 Hz, 1H); 8.52 (d, J = 8.8 Hz, 1H); 12.35 (bs, 1H). ^{13}C NMR (400 MHz, DMSO-d_6, ppm) δ 18.75, 19.38, 21.83, 23.21, 24.66, 31.36, 50.82, 52.19, 57.63, 109.36, 112.42, 121.25, 122.49, 123.61, 127.89, 128.52, 129.58, 130.00, 132.01, 136.28, 147.27, 166.66, 170.83, 173.21, 187.15.

*2-(Phenylindol-3-yl)glyoxyl-(L)-Phenylalanine-(L)-Leucine methyl ester***7.** Yield 69%; mp 95-97 °C; $[\alpha]^{22}_D$ = -36° (c = 2.0 mg/mL in MeOH); ^{1}H NMR (200 MHz, DMSO-d_6, ppm) δ 0.84-0.91 (m, 6H); 1.51-1.53 (m, 2H); 2.72-2.88 (m, 3H); 3.59 (s, 3H); 4.29-4.32 (m, 2H); 7.06-7.49 (m, 11H); 7.75-7.79 (m, 1H); 8.41 (d, J = 6.8 Hz, 1H); 8.76 (d, J = 8.2 Hz, 1H); 12.32 (bs, 1H). ^{13}C NMR (100 MHz, DMSO-d_6, ppm) δ 21.82, 23.22, 24.61, 37.83, 50.78, 52.32, 53.96, 109.38, 112.33, 121.28, 122.50, 123.54, 126.83, 127.79, 128.47, 129.53, 129.83, 129.88, 131.97, 136.23, 137.98, 147.27, 166.15, 171.03, 173.15, 186.80.

2-(Phenylindol-3-yl)glyoxyl-(L)-Phenylalanine-(L)-Isoleucine methyl ester **8**. Yield 71%; mp 97-99 °C; [α]22 D = -32° (c = 2.0 mg/mL in MeOH); 1H NMR (200 MHz, DMSO-d6, ppm) δ 0.85-0.88 (m, 6H); 1.19-1.21 (m, 1H); 1.36-1.46 (m, 1H); 1.75-1.81 (m, 1H); 2.77-2.83 (m, 1H); 2.90-2.95 (m, 1H); 3.62 (s, 3H); 4.23-4.27 (m, 1H); 4.45-4.49 (m, 1H); 7.10-7.14 (m, 1H); 7.22-7.26 (m, 2H); 7.28-7.30 (m, 4H); 7.31-7.34 (m, 2H); 7.40-7.47 (m, 2H); 7.52-7.54 (m, 2H); 7.79 (d, J = 8.0 Hz, 1H); 8.24 (d, J = 8.0 Hz, 1H); 8.73 (d, J = 8.8 Hz, 1H); 12.31 (bs, 1H). ^{13}C NMR (100 MHz, DMSO-d_6, ppm) δ : 11.65, 15.82, 25.26, 36.83, 37.82, 52.12, 53.87, 56.92, 109.38, 112.34, 121.27,

122.53, 123.57, 126.82, 127.77, 128.48, 129.59, 129.84, 129.88, 131.94, 136.21, 137.94, 147.29, 166.21, 171.11, 172.16, 186.83.

General procedure for Boc-deprotection to dipeptide derivatives 101-17. Trifluoracetic acid (4.0 ml) was added to a stirring solution of Boc-dipeptide methyl esters **18**-**24**(0.5 mmol) in DCM (4.0 mL) and the mixture was stirred for 1 h at room temperature. The solvent was removed under reduced pressure and the excess of trifluoracetic acid was co-evaporated with diethyl ether three times to give a white solid which was used in the next reaction without further purification.

$CF_3COO^-{}^+H_3N$-Val-Ile-OMe 11. Yield, quant. ^{1}H NMR (400 MHz, DMSO-d_6) δ 0.83–0.95 (m, 12H); 1.18–1.25 (m, 1H); 1.39–1.46 (m, 1H); 1.77–1.84 (m, 1H); 2.05–2.10 (m, 1H); 3.62 (s, 3H); 3.70 (d, J = 5.3 Hz, 1H); 4.23 (t, J = 5.3 Hz, 1H); 8.10 (br, 1H); 8.58 (d, J = 6.9 Hz, 1H).

$CF_3COO^-{}^+H_3N$-Ile-Val-OMe 12. Yield, quant. ^{1}H NMR (400 MHz, DMSO-d_6) δ 0.83–0.92 (m, 12H); 1.07–1.16 (m, 1H); 1.46–1.52 (m, 1H); 1.78–1.85 (m, 1H); 2.03–2.01 (m, 1H); 3.63 (s, 3H); 3.72 (d, J = 6.1 Hz, 1H); 4.20 (t, J = 7.1 Hz, 1H); 8.01 (br, 1H); 8.50 (d, J = 7.5 Hz, 1H).

$CF_3COO^-{}^+H_3N$-Ile-Ile-OMe 13. Yield: quant. ^{1}H NMR (400 MHz, DMSO-d_6) δ0.81–0.89 (m, 12H); 1.14–1.23 (m, 1H); 1.35–1.49 (m, 2H); 1.73–1.81 (m, 1H); 3.60 (s, 3H); 3.70 (d, J = 4.8 Hz, 1H); 4.35 (br, 1H).

$CF_3COO^-{}^+H_3N$-Leu-Val-OMe 14. Yield: quant. ^{1}H NMR (400 MHz, DMSO-d_6) δ 0.83–0.90 (m, 12H); 1.42–1.53 (m, 2H); 1.60–1.65 (m, 1H); 2.00–2.07 (m, 1H); 3.60 (s, 3H); 3.86 (br, 1H); 4.18 (br, 1H); 8.16 (br, 1H); 8.67 (d, J = 6.9 Hz, 1H). ESI-MS m/z 245.1 (M+H), 272.3 (M+Na^+).

$CF_3COO^-{}^+H_3N$-Val-Leu-OMe 15. Yield: quant. ^{1}H NMR (400 MHz, DMSO-d_6) δ 0.83–0.94 (m, 12H); 1.56–1.64 (m, 3H); 2.03–2.10 (m, 1H); 3.12 (d, J = 5.6 Hz, 1H); 3.29 (br, 1H); 3.60 (s, 3H); 4.28 (br, 1H); 8.07 (br, 1H); 8.68 (br, 1H). ESI-MS m/z 245.3 (M+H).

$CF_3COO^-{}^+H_3NH_2N$-Phe-Leu-OMe 16. Yield: quant. ^{1}H NMR (400 MHz, DMSO-d_6) δ 0.84–0.89 (m, 6H); 1.51–1.57 (m, 2H); 1.59–1.68 (m, 1H); 2.95 (dd, J_1 = 14.0 Hz, J_2 = 6.7 Hz, 1H); 3.10 (dd,

J_1 = 14.0 Hz, J_2 = 8.2 Hz, 1H); 3.61 (s, 3H); 4.06 (d, J = 6.3 Hz, 1H); 4.29-4.33 (m, 1H); 7.25–7.31 (m, 5H); 8.19 (br, 1H); 8.80 (d, J = 7.3 Hz, 1H).

CF3COO-+H$_3$N-Phe-Ile-OMe 17. Yield**:** quant. ^{1}H NMR (400 MHz, DMSO-d$_6$) δ 0.82–0.86 (m, 6H); 1.12–1.22 (m, 1H); 1.38–1.44 (m, 1H); 1.76 (br, 1H); 2.91-2.98 (m, 1H); 3.02-3.09 (m, 1H); 3.61 (s, 3H); 4.08 (m, 1H); 4.22-4.28 (m, 1H); 7.22–7.33 (m, 5H); 8.16 (br, 1H); 8.70 (br, 1H).

General procedure for the synthesis of NH-Boc dipeptide derivatives 18-24. To a solution of the appropriate H_2N-AA-OMe (1 mmol) and the appropriate BocHN-AA-OH (1 mmol) in DMF (4 mL), EDCI (0.230 g, 1.2 mmol) and HOBt·H_2O (0.184 g, 1.2 mmol) were added and the mixture was stirred for 12 h at room temperature. Afterward the reaction was quenched with saturated $NaHCO_3$ solution (30 ml) and the mixture was extracted with ethyl acetate (3 x 30 ml ml). The organic layer was washed with 2N HCl solution (3 x 25 ml), water (3 x 30 ml), brine (3 x 30 ml), dried over anhydrous Na_2SO_4, filtered and concentrated to give pure derivatives **16-21** as white solids.

Boc-HN-Val-Ile-OMe 18. From H_2N-Ile-OMe (0.182 g, 1 mmol) and BocHN-Val-OH (0.217 g, 1 mmol); yield 80%.^{1}H NMR (400 MHz, $CDCl_3$) δ 0.89–0.97 (m, 12H); 1.14–1.24 (m, 2H); 1.44 (s, 9H); 1.87-1.93 (m, 1H); 2.07-2.18 (br, 1H); 3.73 (s, 3H); 3.90 (t, J = 14.9 Hz, 1H); 4.58 (dd, J_1 = 13.4 Hz, J_2 = 3.6 Hz, 1H); 5.04 (d, J = 5.9 Hz, 1H); 6.38 (d, J = 6.3 Hz, 1H).

Boc-Ile-Val-OMe 19. From H_2N-Val-OMe (0.131 g, 1 mmol) and BocHN-Ile-OH (0.231 g, 1 mmol); yield 69%.^{1}H NMR (400 MHz, $CDCl_3$) δ 0.90–0.96 (m, 12H); 1.10–1.19 (m, 1H); 1.49-1.65 (m, 3H); 1.83-1.90 (m, 1H); 2.14-2.22 (br, 1H); 3.73 (s, 3H); 3.93 (t, J = 8.2 Hz, 1H); 4.54 (dd, J_1= 8.7 Hz, J_2 = 3.8 Hz, 1H); 5.01 (br, 1H); 6.38 (d, J = 5.8 Hz, 1H).

Boc-HN-Ile-Ile-Ome 20. From H_2N-Ile-OMe (0.182 g, 1 mmol) and BocHN-Ile-OH (0.231 g, 1 mmol); yield 78%.^{1}H NMR (400 MHz, $CDCl_3$) δ 0.89–0.94 (m, 12H); 1.06–1.24 (m, 2H); 1.43 (s,

9H); 1.80–1.95 (m, 2H); 1.64 (br, 1H); 1.80–1.89 (m, 1H); 3.73 (s, 3H); 3.93 (t, J = 15.1 Hz, 1H); 4.58 (dd, J_1 = 13.4 Hz, J_2 = 3.6 Hz, 1H); 5.04 (d, J = 6.4 Hz, 1H); 6.38 (d, J = 7.2 Hz, 1H).

Boc-HN-Leu-Val-OMe 21. From H_2N-Val-OMe (0.131 g, 1 mmol) and BocHN-Ile-OH (0.231 g, 1 mmol); yield 69%.^{1}H NMR (400 MHz, $CDCl_3$) δ 0.89–0.95 (m, 12H); 1.44 (s, 9H); 1.60-1.68 (m, 3H); 2.13-2.20 (m, 1H); 3.73 (s, 3H); 4.1 (br, 1H); 4.53 (dd, J_1 = 8.8 Hz, J_2 = 3.9 Hz, 1H); 4.84 (br, 1H); 6.55 (d, J = 7.6 Hz, 1H).

Boc-HN-Val-Leu-OMe 22. From H_2N-Leu-OMe (0.182 g, 1 mmol) and BocHN-Val-OH (0.217 g, 1 mmol); yield 92%.^{1}H NMR (400 MHz, $CDCl_3$) δ 0.91–0.97 (m, 12H); 1.43 (s, 9H); 1.52-1.68 (m, 3H); 2.00-2.18 (br, 1H); 3.71 (s, 3H); 3.88 (t, J = 15.0 Hz, 1H); 4.59-4-64 (m, 1H); 5.06 (d, J = 7.0 Hz, 1H); 6.28 (d, J = 4.7 Hz, 1H).

Boc-HN-Phe-Leu-OMe 23. From H_2N-Leu-OMe (0.182 g, 1 mmol) and BocHN-Phe-OH (0.265 g, 1 mmol); yield 77%.^{1}H NMR (400 MHz, $CDCl_3$) δ 0.89 (t, J = 6.5 Hz, 6H); 1.41 (s, 9H); 1.52-1.62 (m, 3H); 3.07 (d, J = 6.4 Hz, 1H); 3.69 (s, 3H); 3.90 (t, J = 14.9 Hz, 1H); 4.31-4.37 (m, 1H); 4.53-4.59 (m, 1H); 4.99 (br, 1H); 6.22 (d, J = 8.0 Hz, 1H); 7.20-7.31 (m, 5H).

Boc-HN-Phe-Ile-OMe 24. From H_2N-Leu-OMe (0.182 g, 1 mmol) and BocHN-Phe-OH (0.265 g, 1 mmol); yield 85%. ^{1}H NMR (400 MHz, $CDCl_3$) δ 0.82-0.90 (m, 6H); 1.06-1.13 (m, 1H); 1.32-1.39 (m, 1H); 1.42 (s, 9H); 1.83 (br, 1H); 3.05-3.09 (m, 1H); 3.69 (s, 3H); 4.33 (br, 1H); 4.48-4.52 (m, 1H); 5.00 (br, 1H); 6.35 (d, J = 6.5 Hz, 1H); 7.20-7.31 (m, 5H).

Biological Studies.

Dissociation studies of native MDM2/p53 complex. To test the ability of new compound to dissociate the native MDM2/p53 complex, a quantitative sandwich immune-enzymatic assay, on crude cell lysates obtained from U87MG cells was used, as previously described.[21] In brief, U87MG cell were suspended in lysis buffer (20 mM Tris HCl, 137 mM NaCl, 10% glycerol, 1% NONIDET40, 2 mM EDTA, pH 8) containing 1% of the Protease inhibitor Cocktail (Sigma

Aldrich, Milan, Italy). Cell lysates (15 μg in a final volume of 100 μl) were pre-incubated with DMSO (control) or different compound concentration for 10 minutes at room temperature, and then transferred for 60 min to wells pre-coated with a mouse full-length anti-MDM2 antibody (sc-965, Santa Cruz Biotechnology, 1:50 in 0.05% Poly-L-Ornithine, overnight at room temperature). After three quick washes with PBS/Tween 0.05% to remove unbound MDM2, each well was incubated for 15 min with 1% BSA, to block nonspecific sites, and then for 1.5 h at room temperature with a rabbit primary anti-p53 antibody (sc-6243, Santa Cruz Biotechnology, 1:250 in 5% milk). Then, wells were washed and incubated for 1 h with an anti-rabbit HRP-conjugate antibody (1:3000 in 5% milk), and washed again. The TMB substrate kit (Thermo Fisher Scientific) allowed a colorimetric quantification of the MDM2/p53 complex. Blanks were obtained processing cell lysates in the absence of the primary anti-p53 antibody. Absorbance's values at 450 nm were measured, background subtracted and sigmoid dose-response curves were generated using Graph Pad Prism 5 software, from which IC_{50} values of MDM2/p53 complex were derived.

p53 stabilization analysis in U87MG cells. The western blot analysis for the evaluation of p53 protein levels was performed as previously described.[37] In brief, U87MG cells were treated with DMSO (control) or 1 μM **1**, or 1 μM **7** or 10 μM Nutlin-3 for 8 h , and then lysed for 60 min at 4 °C by the addition of 200 μl RIPA buffer (9.1 mM NaH_2PO_4, 1.7 mM Na_2HPO_4, 150 mM NaCl, pH 7.4, 0.5% sodium deoxycholate, 1% Nonidet P-40, and 0.1% SDS, protease inhibitor cocktail). Equal amount of the cell extracts (40 μg of proteins) were diluted in Laemmli solution, resolved by SDS-PAGE (8.5%), transferred to PVDF membranes and probed overnight at 4 °C with primary antibody anti-p53 (FL-393, rabbit polyclonal antibody raised against amino acids 1-393 mapping at the C-terminus of p53 of human origin; Santa Cruz Biotechnology; 1:500). The primary antibody was detected using anti-rabbit IgG light chains conjugated to peroxidase (diluted 1:10.000). The peroxidase was detected using a chemioluminescent substrate (ECL, Perkin Elmer). Densitometric analysis of immunoreactive bands was performed using Image J Software.

Competitive [^{3}H]PK11195 radioligand binding assay. Binding studies were performed as previously described.[25] Briefly, crude mitochondrial membranes, in 50 mM Tris-HCl pH 7.4 buffer, were incubated with 0.5 nM [^{3}H]PK11195 in the presence of new synthesized compounds (0.04 nM-400 μM) in a final volume of 0.5 ml for 90 min at 4 °C. Incubations were terminated by rapid filtration through GF/C glass fiber filters and washed three times with 4 ml of cold buffer. The radioactivity was measured by liquid scintillation counter. Non-specific binding was estimated in the presence of unlabeled 1 μM PK11195. IC_{50} value was determined using the non-linear multipurpose curve-fitting Graph-Pad Prism computer program (Graph Pad Prism Software, version 5.0; San Diego, CA).

Cell culture and CSC isolation. The human glioblastoma multiforme U87MG, T98G and U343MG cell lines were obtained from the National Institute for Cancer Research of Genoa (Italy), American Type Culture Collection (USA) and Cell Lines Service GmbH (Germany), respectively. Each cell line was monitored for DNA profiling. The U87MG and T98G cells were cultured in RPMI medium supplemented with 10% FBS, 2 mM L-glutamine, 100 U/ml penicillin, 100 mg/ml streptomycin and 1% non-essential amino acids at 37 °C in 5% CO_2. The U343MG cells were cultured in Minimum essential medium Eagle with 2 mM Lglutamine and Earle's BSS adjusted to contain 1.5 g/l sodium bicarbonate and supplemented with 10% FBS, 100 U/ml penicillin, 100 mg/ml streptomycin, 1% non-essential amino acids and 1.0 mM sodium pyruvate at 37°C in 5% CO_2.

To isolate GSCs, approximately 2.0 x 10^6 cells were suspended in 1 mL of a defined serum-free Neural Stem Cell (NSC) medium.[8] After 3-4 days of culture, the neurospheres were collected, suspended in NSC medium, dissociated into single cells, and plated for the assays. For the long-term treatment of cells, NSC or complete medium containing drugs was replaced every two to three days.

Human MSCs were cultured in normal growth medium (MSCGM, Lonza), plated ($5X10^3$ cells/cm^2) in 75-cm^2 flasks and incubated at 37 °C in 5% CO_2 and 95% air. The medium was changed to remove non adherent cells every 3 to 4 days, and the cells were used at passages 0 to 3.

Annexin V and 7-AAD staining in U87MG cells. Dual staining with Annexin V coniugated to fluorescein-isothiocyanate (FITC) and 7-amino-actinomysin (7-AAD) was performed using the commercially available kit (Muse Annexin V and Dead Cell Kit; Merck KGaA, Darmstadt, Germany). U87MG cells were treated with DMSO (control) or 1 μM **1** or 1 μM **7** for 24 h. At the end of the treatment periods, both floating and adherent cells were collected, centrifuged at 300 x g for 5 min and suspended in cell culture medium. Then, a 100 μl aliquot of cell suspension (about $5x10^4$ cell/ml) was added to 100 μl of fluorescent reagent and incubated for 10 min at room temperature. After incubation, the percentages of living, apoptotic and dead cells were acquired and analyzed by Muse™ Cell Analyzer in accordance to the manufacture's guidelines. In cells undergoing apoptosis, annexin V binds to phosphatidylserine, which is translocated from the inner to the outer leaflet of the cytoplasmatic membrane. Double staining is used to distinguish between viable, early apoptotic,and necrotic or late apoptotic cells.Annexin V: FITC positive and 7-AAD positive cells were identified as early apoptotic. Cells which were Annexin V-FITC positive and 7-AAD positive were identified as cells in late apoptosis or necrotic.

Cell cycle analysis in U87MG cells. The measurement of the percentage of cells in the different cell phases was performed using the Muse™ Cell Analyzer, Merck KGaA, Darmstadt, Germany). Briefly, U87MG cells were treated for 24 h with DMSO or 1 μM **7**. Adherent cells were collected and centrifuged at 300 x g for 5 min. The pellet was washed with PBS and suspended in 100 μl of PBS; finally cells were slowly added to 1 ml of ice cold 70% ethanol and maintained o/n at –20 °C. Then, a cell suspension aliquot (containing at least $2x10^5$ cells) was centrifuged at 300 x g for 5 min, washed once with PBS and suspended in the fluorescent reagent (Muse™ Cell Cycle reagent).

After incubation for 30 min at room temperature in the dark, the measurements of the percentage of cells in the different phases was acquired.

RNA extraction and Real Time PCR analysis in U87MG cells. U87MG cells were treated for 6 h with DMSO or 1 μM **1** or 1 μM **7**. At the end of treatments, cells were collected, and total RNA was extracted using Rneasy® Mini Kit (Qiagen, Hilden, Germany) according to manufacturer's instructions. cDNA synthesis was performed with 500 ng of RNA using i-Script cDNA synthesis kit (BioRad, Hercules, USA) following manufacturer's instructions. RT-PCR reactions consisted of 25 μL Fluocycle® II SYBR® (Euroclone, Milan, Italy), 1.5 μL of both 10 μM forward and reverse primers, 3 μL cDNA, and 19 μL of H_2O. All reactions were performed for 40 cycles using the following temperature profiles: 98 °C for 30 seconds (initial denaturation); T °C for 30 seconds (annealing); and 72 °C for 3 seconds (extension). The primer sequences and annealing temperature were chosen as reported previously.[31,40]

Cell viability assay. U87MG cells, U343MG or T98G were plated at a density of 3,000 cells/well. CSCs or MSCs were plated at a density of 10,000 cells/well. After 24 h, the culture medium was replaced with fresh medium containing compound 1, **7**, Nutlin-3 or PK11195 solubilized in DMSO for the indicated times. In co-treatment experiments, U87MG or CSCs were treated with 100 nM **7** in the presence or absence or 50 μM TMZ. Following incubation time, cell viability was determined using the MTS assay according to manufacturer's instruction. The dehydrogenase activity in active mitochondria reduces 3-(4,5-dimethylthiazol-2-yl)-5-(3-carboxymethoxyphenyl)-2-(4-sulfophenyl)-2H-tetrazolium (MTS) to the soluble formazan product. The absorbance of formazan at 490 nM was measured in a colorimetric assay with an automated plate reader (Victor Wallac 2, Perkin Elmer). Each cell treatment was assayed in triplicate, and each experiment was performed at least three times. The results were calculated by subtracting the mean background from the values obtained from each evaluation and were expressed as the percentage of the control (untreated cells). Sigmoid dose-response curves were generated from which the IC_{50} values were derived.

Molecular Modeling. MDM2 structure selection. Several 3D structures of MDM2 can be found in the Protein Data Bank (PDB). Among them we took in consideration just the ones containing the N-terminus residues 16-24 (eg. 3LBL, 4HBM, 4DIJ, 4JVR, 4JVE, 1T4E, 4ERF, etc.) which forms an ordered helix that modifies shape and size of the catalytic pocket and provides further points of interactions. Thus, among the non-truncated X-ray structures containing an organic compound, the one with the highest resolution (PDB code 3LBL, 1.60 Å) cocrystallized with a spirooxindole derivative was selected for docking studies. The binding modes of compound **7** were studied by means of docking experiments with the widely-used Glide5.5 software in extra precision (XP) mode, using Glidescore for ligand ranking.[32] The ligands 3D structures were created with the Maestro Build Panel.[37] The target MDM2 structure was prepared through the Protein Preparation Wizard within the Maestro 9.0.2112 package using the OPLS-2001 force field.

The same docking procedure was used to dock **1**, **7** and **8** in the homology built structure of the rat TSPO structure. The homology building procedure is reported in our previous work.[33]

Figures 1 and 6 were rendered using the Chimera software package.[41]

AUTHOR INFORMATION

Corresponding Author:

* Luciana Marinelli e-mail: lmarinel@unina.it; Sabrina Taliani e-mail: sabrina.taliani@farm.unipi.it

Author Contributions

The manuscript was written through contributions of all authors. All authors have given approval to the final version of the manuscript.

Funding Sources

This work was supported by the FIRB, Bando Futuro in Ricerca 2010 (Grant RBFR10ZJQT).

Notes

Any additional relevant notes should be placed here.

ACKNOWLEDGMENT

The research program was funded by FIRB-Programma“Futuro in Ricerca” RBFR10ZJQT.

ABBREVIATIONS

7-AAD, 7-Amino-actinomysin;CNS, central nervous system; CSCs, cancer stem cells; FITC,fluorescein-isothiocyanate; GBM, Glioblastoma multiforme; MDM, murine double minute;MOMP,Mitochondrial Outer Membrane Permeabilization;MTS, 3-(4,5-dimethylthiazol-2-yl)-5-(3-carboxymethoxyphenyl)-2-(4-sulfophenyl)-2H-tetrazolium; PDB,Protein Data Bank;TMZ, temozolomide.

Insert Table of Contents Graphic and Synopsis Here

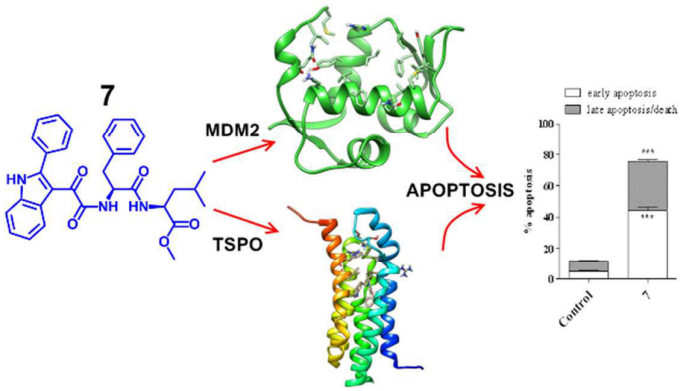

REFERENCES

1. Ostrom, Q. T.; Gittleman, H.; Farah, P.; Ondracek, A.; Chen, Y.; Wolinsky, Y.; Stroup, N. E.; Kruchko, C.; Barnholtz-Sloan, J. S. CBTRUS statistical report: Primary brain and central nervous system tumors diagnosed in the United States in 2006-2010. *Neuro Oncol.***2013**, *15*, ii1-56.

2. Lacroix, M.; Abi-Said, D.; Fourney, D. R.; Gokaslan, Z. L.; Shi, W.; DeMonte, F.; Lang, F. F.; McCutcheon, I. E.; Hassenbusch, S. J.; Holland, E.; Hess, K.; Michael, C.; Miller, D.; Sawaya, R. A multivariate analysis of 416 patients with glioblastoma multiforme: prognosis, extent of resection, and survival. *J. Neurosurg.***2001**,*95*, 190-198.

3. Stupp, R.; Mason, W. P.; van den Bent, M. J.; Weller, M.; Fisher, B.; Taphoorn, M. J.; Belanger, K.; Brandes, A. A.; Marosi, C.; Bogdahn, U.; Curschmann, J.; Janzer, R. C.; Ludwin, S. K.; Gorlia, T.; Allgeier, A.; Lacombe, D.; Cairncross, J. G.; Eisenhauer, E.; Mirimanoff, R. O. Radiotherapy plus concomitant and adjuvant temozolomide for glioblastoma. *N. Engl. J. Med.***2005**,*352*, 987-996.

4. Gilbert, M. R.; Dignam, J. J.; Armstrong, T. S.; Wefel, J. S.; Blumenthal, D. T.; Vogelbaum, M. A.; Colman, H.; Chakravarti, A.; Pugh, S.; Won, M.; Jeraj, R.; Brown, P. D.; Jaeckle, K. A.; Schiff, D.; Stieber, V. W.; Brachman, D. G.; Werner-Wasik, M.; Tremont-Lukats, I. W.; Sulman, E. P.; Aldape, K. D.; Curran, W. J.; Mehta, M. P. A randomized trial of bevacizumab for newly diagnosed glioblastoma. *N. Engl. J. Med.***2014**,*370*, 699-708.

5. Carlsson, S. K.; Brothers, S. P.; Wahlestedt, C. Emerging treatment strategies for glioblastoma multiforme. *EMBO Mol. Med.***2014**, *6*, 1359-1370.

6. Eramo, A.; Ricci-Vitiani, L.; Zeuner, A.; Pallini, R.; Lotti, F.; Sette, G.; Pilozzi, E.; Larocca, L. M.; Peschle, C.; De Maria, R. Chemotherapy resistance of glioblastoma stem cells. *Cell Death Differ.***2006**,*13*, 1238-1241.

7. Smalley, M.; Piggott, L.; Clarkson, R. Breast cancer stem cells: obstacles to therapy. *Cancer Lett.***2013**,*338*, 57-62.

8. Daniele, S.; Zappelli, E.; Natali, L.; Martini, C.; Trincavelli, M. L. Modulation of A1 and A_{2B} adenosine receptor activity: a new strategy to sensitise glioblastoma stem cells to chemotherapy. *Cell Death Dis.***2014**,*5*, e1539.

9. Tait, S. W.; Green, D. R. Mitochondria and cell death: outer membrane permeabilization and beyond. *Nat. Rev. Mol. Cell. Biol.***2010**,*11*, 621-632.

10. Fulda, S.; Galluzzi, L.; Kroemer, G. Targeting mitochondria for cancer therapy. *Nat. Rev. Drug Discov.***2010**, *9*, 447-464.

11. Stornaiuolo, M.; La Regina, G.; Passacantilli, S.; Grassia, G.; Coluccia, A.; La Pietra, V.; Giustiniano, M.; Cassese, H.; Di Maro, S.; Brancaccio, D.; Taliani, S.; Ialenti, A.; Silvestri, R.; Martini, C.; Novellino, E.; Marinelli, L. Structure-Based Lead Optimization and Biological Evaluation of BAX Direct Activators as Novel Potential Anticancer Agents. *J. Med. Chem.***2015**, *58*, 2135-2148.

12. Griguer, C. E.; Oliva, C. R. Bioenergetics pathways and therapeutic resistance in gliomas: emerging role of mitochondria. *Curr. Pharm. Des.***2011**,*17*, 2421-2427.

13. Mathupala, S. P.; Pedersen, P. L. Voltage dependent anion channel-1 (VDAC-1) as an anti-cancer target. *Cancer Biol. Ther.***2010**,*9*, 1053-1056.

14. Austin, C. J.; Kahlert, J.; Kassiou, M.; Rendina, L. M. The translocator protein (TSPO): a novel target for cancer chemotherapy. *Int. J. Biochem. Cell. Biol.***2013**,*45*, 1212-1216.

15. Papadopoulos, V.; Baraldi, M.; Guilarte, T. R.; Knudsen, T. B.; Lacapere, J. J.; Lindemann, P.; Norenberg, M. D.; Nutt, D.; Weizman, A.; Zhang, M. R.; Gavish, M. Translocator protein (18kDa): new nomenclature for the peripheral-type benzodiazepine receptor based on its structure and molecular function. *Trends Pharmacol. Sci.***2006**,*27*, 402-409.

16. Mendonca-Torres, M. C.; Roberts, S. S. The translocator protein (TSPO) ligand PK11195 induces apoptosis and cell cycle arrest and sensitizes to chemotherapy treatment in pre- and post-relapse neuroblastoma cell lines. *Cancer Biol. Ther.***2013**, *14*, 319-326.

17. Plescia, J.; Salz, W.; Xia, F.; Pennati, M.; Zaffaroni, N.; Daidone, M. G.; Meli, M.; Dohi, T.; Fortugno, P.; Nefedova, Y.; Gabrilovich, D. I.; Colombo, G.; Altieri, D. C. Rational design of shepherdin, a novel anticancer agent. *Cancer Cell* **2005**,*7*, 457-468.

18. Chelli, B.; Rossi, L.; Da Pozzo, E.; Costa, B.; Spinetti, F.; Rechichi, M.; Salvetti, A.; Lena, A.; Simorini, F.; Vanacore, R.; Scatena, F.; Da Settimo, F.; Gremigni, V.; Martini, C. PIGA (*N*,*N*-Di-*n*-butyl-5-chloro-2-(4-chlorophenyl)indol-3-ylglyoxylamide), a new mitochondrial benzodiazepine-receptor ligand, induces apoptosis in C6 glioma cells. *Chembiochem* **2005**,*6*, 1082-1088.

19. Castellano, S.; Taliani, S.; Milite, C.; Pugliesi, I.; Da Pozzo, E.; Rizzetto, E.; Bendinelli, S.; Costa, B.; Cosconati, S.; Greco, G.; Novellino, E.; Sbardella, G.; Stefancich, G.; Martini, C.; Da Settimo, F. Synthesis and biological evaluation of 4-phenylquinazoline-2-carboxamides designed as a novel class of potent ligands of the translocator protein. *J. Med. Chem.***2012**,*55*, 4506-4510.

20. Castellano, S.; Taliani, S.; Viviano, M.; Milite, C.; Da Pozzo, E.; Costa, B.; Barresi, E.; Bruno, A.; Cosconati, S.; Marinelli, L.; Greco, G.; Novellino, E.; Sbardella, G.; Da Settimo, F.; Martini, C. Structure-activity relationship refinement and further assessment of 4-phenylquinazoline-2-carboxamide translocator protein ligands as antiproliferative agents in human glioblastoma tumors. *J. Med. Chem.***2014**,*57*, 2413-2428.

21. Daniele, S.; Taliani, S.; Da Pozzo, E.; Giacomelli, C.; Costa, B.; Trincavelli, M. L.; Rossi, L.; La Pietra, V.; Barresi, E.; Carotenuto, A.; Limatola, A.; Lamberti, A.; Marinelli, L.; Novellino, E.; Da Settimo, F.; Martini, C. Apoptosis therapy in cancer: the first single-molecule co-activating p53 and the translocator protein in glioblastoma. *Sci. Rep.***2014**, *4*, 4749.

22. Liu, G.; Yuan, X.; Zeng, Z.; Tunici, P.; Ng, H.; Abdulkadir, I. R.; Lu, L.; Irvin, D.; Black, K. L.; Yu, J. S. Analysis of gene expression and chemoresistance of CD133+ cancer stem cells in glioblastoma. *Mol. Cancer* **2006**,*5*, 67.

23. Frank, N. Y.; Schatton, T.; Frank, M. H. The therapeutic promise of the cancer stem cell concept. *J. Clin. Invest.***2010**,*120*, 41-50.

24. Michelsen, K.; Jordan, J. B.; Lewis, J.; Long, A. M.; Yang, E.; Rew, Y.; Zhou, J.; Yakowec, P.; Schnier, P. D.; Huang, X.; Poppe, L. Ordering of the N-terminus of human MDM2 by small molecule inhibitors. *J. Am. Chem. Soc.***2012**, *134*, 17059-17067.

25. Primofiore, G.; Da Settimo, F.; Taliani, S.; Simorini, F.; Patrizi, M. P.; Novellino, E.; Greco, G.; Abignente, E.; Costa, B.; Chelli, B.; Martini, C.*N*,*N*-dialkyl-2-phenylindol-3-ylglyoxylamides. A new class of potent and selective ligands at the peripheral benzodiazepine receptor. *J. Med. Chem.***2004,***47*, 1852-1855.

26. Da Settimo, F.; Simorini, F.; Taliani, S.; La Motta, C.; Marini, A. M.; Salerno, S.; Bellandi, M.; Novellino, E.; Greco, G.; Cosimelli, B.; Da Pozzo, E.; Costa, B.; Simola, N.; Morelli, M.; Martini, C. Anxiolytic-like effects of *N*,*N*-dialkyl-2-phenylindol-3-ylglyoxylamides by modulation of translocator protein promoting neurosteroid biosynthesis. *J. Med. Chem.***2008**,*51*, 5798-5806.

27. Taliani, S.; Simorini, F.; Sergianni, V.; La Motta, C.; Da Settimo, F.; Cosimelli, B.; Abignente, E.; Greco, G.; Novellino, E.; Rossi, L.; Gremigni, V.; Spinetti, F.; Chelli, B.; Martini, C. New fluorescent 2-phenylindolglyoxylamide derivatives as probes targeting the peripheral-type benzodiazepine receptor: design, synthesis, and biological evaluation. *J. Med. Chem.***2007**,*50*, 404-407.

28. Taliani, S.; Da Pozzo, E.; Bellandi, M.; Bendinelli, S.; Pugliesi, I.; Simorini, F.; La Motta, C.; Salerno, S.; Marini, A. M.; Da Settimo, F.; Cosimelli, B.; Greco, G.; Novellino, E.; Martini, C., Novel irreversible fluorescent probes targeting the 18 kDa translocator protein: synthesis and biological characterization. *J. Med. Chem.***2010**,*53*, 4085-4093.

29. Costa, B. ; Da Pozzo, E.; Giacomelli, C.; Taliani, S.; Bendinelli, S.; Barresi, E.; Da Settimo, F.; Martini, C. TSPO ligand residence time influences human glioblastoma multiforme cell death/life balance.*Apoptosis* **2015**, *20*, 383-398.

30. Wang, S.I.; Puc, J.; Li, J.; Bruce, J.N.; Cairns, P.; Sidransky, D.; Parsons R. Somatic mutations of PTEN in glioblastoma multiforme. *Cancer Res.* **1997**, *57*, 4183-4186.

31. Daniele, S.; Costa, B.; Zappelli, E.; Da Pozzo, E.; Sestito, S.; Nesi, G.; Campiglia, P.; Marinelli, L.; Novellino, E.; Rapposelli, S.; Martini, C. Combined inhibition of AKT/mTOR and MDM2 enhances Glioblastoma Multiforme cell apoptosis and differentiation of cancer stem cells. *Sci. Rep.* **2015**, *5*, 9956.

32. Glide, version 5.5; Schrodinger, LLC: New York. **2009**.

33. Barresi, E.; Bruno, A.; Taliani, S.; Cosconati, S.; Da Pozzo, E.; Salerno, S.; Simorini, F.; Daniele, S.; Giacomelli, C.; Marini, A.M.; La Motta, C.; Marinelli, L.; Cosimelli, B.; Novellino, E.; Greco, G.; Da Settimo, F.; Martini, C. Deepening the Topology of the Translocator Protein Binding Site by Novel N,N-Dialkyl-2-arylindol-3-ylglyoxylamides. *J. Med. Chem.***2015**, *58*, 6081-6092.

34. Chelli, B.; Salvetti, A.; Da Pozzo, E.; Rechichi, M.; Spinetti, F.; Rossi, L.; Costa, B.; Lena, A.; Rainaldi, G.; Scatena, F.; Vanacore, R.; Gremigni, V.; Martini, C. PK 11195 differentially affects cell survival in human wild-type and 18 kDa translocator protein-silenced ADF astrocytoma cells. *J. Cell. Biochem.* **2008**, *105*, 712-723.

35. Wang, C.C.; Liao, Y.P.; Mischel, P.S.; Iwamoto, K.S.; Cacalano, N.A,; McBride, W.H. HDJ-2 as a target for radiosensitization of glioblastoma multiforme cells by the farnesyltransferase inhibitor R115777 and the role of the p53/p21 pathway. *Cancer Res.* **2006**, *66,* 6756-6762.

36. Gabelloni, P.; Da Pozzo, E.; Bendinelli, S.; Costa, B.; Nuti, E.; Casalini, F.; Orlandini, E.; Da Settimo, F.; Rossello, A.; Martini, C. Inhibition of metalloproteinases derived from tumours: new insights in the treatment of human glioblastoma. *Neuroscience*. **2010**, *168*, 514-522.

37. Schrodinger, L. L. C., Maestro, Version 9.0.211, New York, NY. **2009**.

38. Patel, T.; Zhou, J.; Piepmeier, J.M.; Saltzman, W.M. *Adv. Drug Deliv. Rev.* **2012,** 64, 701–705.

39. Pardridge, W.M.; Boado, R.J. Reengineering biopharmaceuticals for targeted delivery across the blood-brain barrier. *Methods Enzymol.* **2012**, 503, 269–292

40. Costa, B.; Bendinelli, S.; Gabelloni, P.; Da Pozzo, E.; Daniele, S.; Scatena, F.; Vanacore, R.; Campiglia, P.; Bertamino, A.; Gomez-Monterrey, I.; Sorriento, D.; Del Giudice, C.; Iaccarino, G.;

Novellino, E.; Martini, C. Human glioblastoma multiforme: p53 reactivation by a novel MDM2 inhibitor. *PLoS One* **2013,***8*, e72281.

41. Pettersen, E. F.; Goddard, T. D.; Huang, C. C.; Couch, G. S.; Greenblatt, D. M.; Meng, E. C.; Ferrin, T. E. UCSF Chimera--a visualization system for exploratory research and analysis. *J. Comput. Chem.***2004**,*25*, 1605-1612.

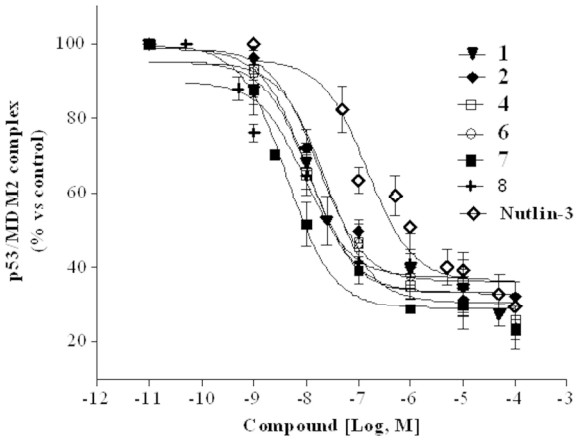

ELISA-based in vitro MDM2/p53 protein-protein interaction assay. U87MG cell lysates, containing the native MDM2/p53 complex, were pre-incubated with DMSO (control) or different concentrations of the selected compounds. Then, MDM2 contained in lysate, alone and bound to p53, was captured on MDM2 antibody pre-coated wells. After extensive washes, an antibody specific for p53 was added to the wells and incubated for 90 minutes. The levels of the MDM2/p53 complex were quantified using an HRP-conjugated antibody and a TMB substrate kit. Blank wells were obtained in the absence of p53 antibody. The data were expressed as a percentage with respect to that of untreated cells (control), which was set to 100%, and they are the mean ± SEM of at least three independent experiments. Curves were generated using a sigmoidal dose-response curve model (GraphPad Prism 5 software) from which the IC50 values were derived.
190x142mm (300 x 300 DPI)

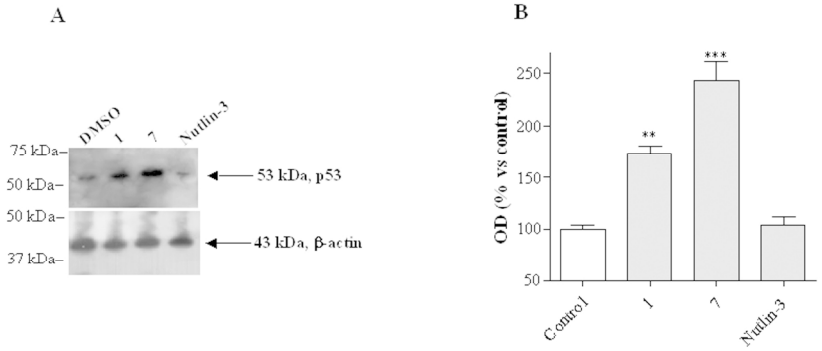

p53 protein accumulation in U87MG cells. The U87MG cells were treated with DMSO (Control), 1 μM 1, 1 μM 7 or 10 μM Nutlin-3 for 8 h. Lysates were subjected to Western blot analysis using antibody to p53 (FL-393; Santa Cruz Biotechnology). One representative Western blot is presented (panel A) for each cell treatment. β-actin was the loading control. The bar graph (panel B) shows the quantitative analysis of the Western blots, performed using ImageJ. The data were expressed as the percentage of Optical Density (OD) versus control set to 100%, and are the mean ± SEM of three different experiments. Statistical significance was determined with a one-way ANOVA with Bonferroni post-test: **P<0.01, ***P<0.001 vs Control.
190x142mm (300 x 300 DPI)

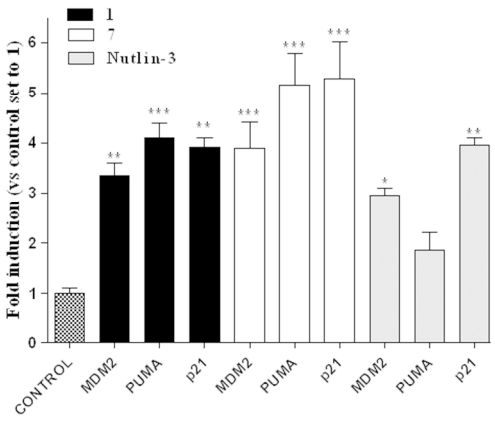

Transcription of p53 target genes in U87MG cells. U87MG cells were treated with DMSO (Control), 1 μM 1, 1 μM 7 or 10 μM Nutlin-3 for 6 h. The relative mRNA quantification of p53 target genes (PUMA, p21 and MDM2) was performed by real-time RT-PCR as describe in the Methods section. The data were expressed as the fold change versus the levels of the control, and are the mean values ± SEM of three different experiments, each performed in duplicate. The significance of the differences was determined with a one-way ANOVA with Bonferroni post-test: *P<0.05, **P<0.01, *** P<0.001 vs control.
190x142mm (300 x 300 DPI)

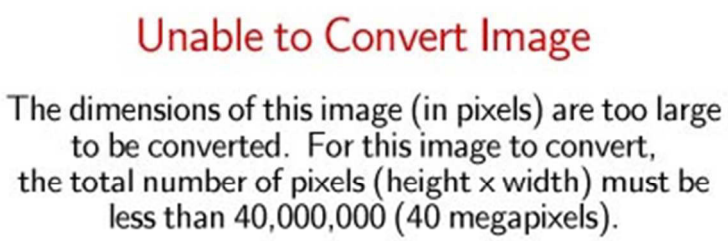

(a) Binding mode of compound 7 in the rat TSPO homology model structure. The ligand is represented as coral sticks while the receptor as cyan sticks and ribbons. (b) Manually docked binding pose of compound 1 in the rat TSPO homology model structure. The ligand is represented as coral sticks while the receptor as cyan sticks and ribbons and white spheres to outline restricted receptor regions.

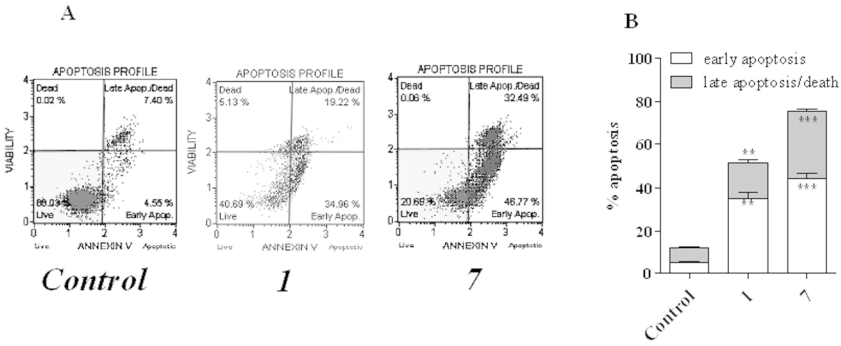

U87MG cell apoptosis. U87MG cells were treated for 24 h with DMSO (control), 1 μM 1 or 1 μM 7. At the end of the treatment periods, the cells were collected and the level of phosphatidylserine externalisation was evaluated using the Annexin V-staining protocol, as described in the Methods section. b) The data were expressed as the percentage of apoptotic cells (data for the early-stage apoptotic cells shown in white and data for the late-stage apoptotic/necrotic cells shown in grey) versus the total number of cells. The data are the mean ± SEM of three different experiments. The significance of the differences was determined with a one-way ANOVA with Bonferroni post-test: ** P<0.01, *** P<0.001 vs control.
190x142mm (300 x 300 DPI)

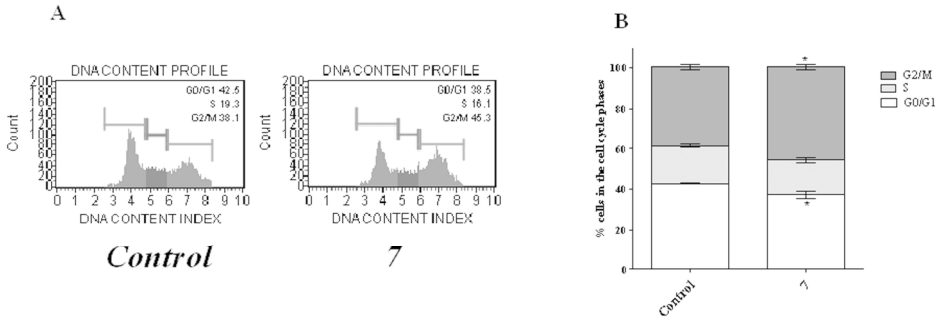

U87MG cells were treated for 24h with DMSO (Control), or 1 μM 7. At the end of the treatment periods, cell cycle was analysed as described in the Methods section. Representative cell cycle histograms of untreated and treated cells were shown (A). The data were expressed as percentage of cell in the different phases (G0/G1, G2 or S) versus total cell number, and they are the mean values ± SEM of three different experiments. The significance of the differences was determined with a one-way ANOVA with Bonferroni post-test: * $P<0.05$ vs control in the respective cellular phase.
190x142mm (300 x 300 DPI)

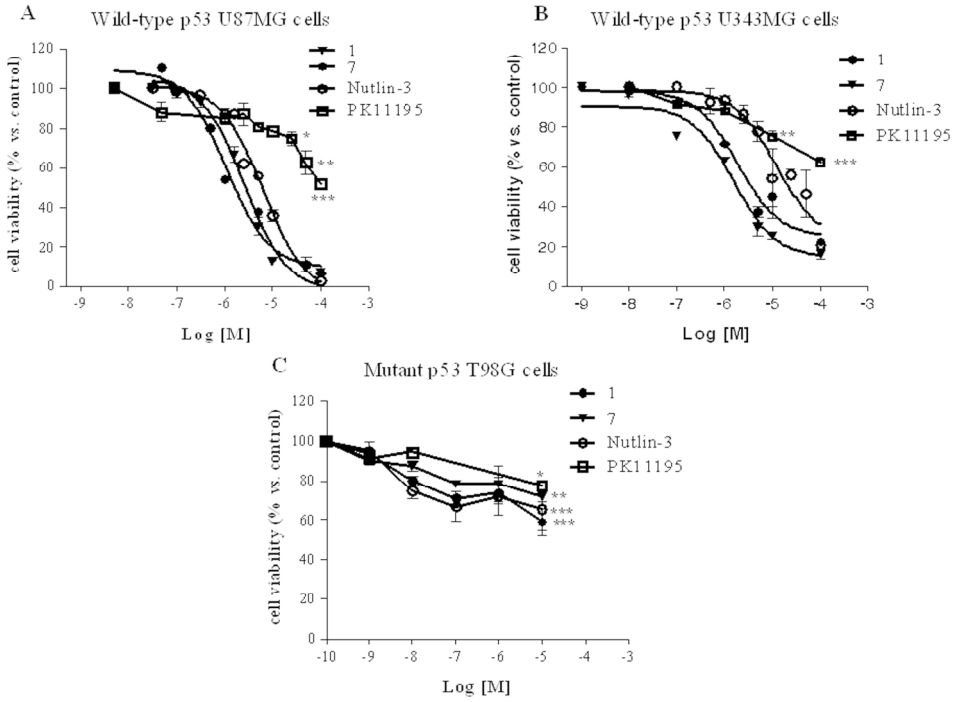

Evaluation of in vitro anti-proliferative effect. U87MG (A), U343MG (B) or T98G (C) cells were incubated with increasing concentrations of 1, 7, Nutlin-3 or PK11195, and cell viability was assessed after 48 h of treatment by MTS assay. The data were expressed as a percentage with respect to that of untreated cells (control), which was set to 100%. Curves were generated using a sigmoidal dose-response curve model (GraphPad Prism 5 software), from which the IC50 values were derived. The data were expressed as a percentage with respect to that of untreated cells (control), which was set to 100%, and are the mean values ± SEM of three independent experiments, each performed in duplicate. The significance of the differences was determined with a one-way ANOVA with Bonferroni post-test: * P<0.05, ** P<0.01, *** P<0.001 vs control.
190x142mm (300 x 300 DPI)

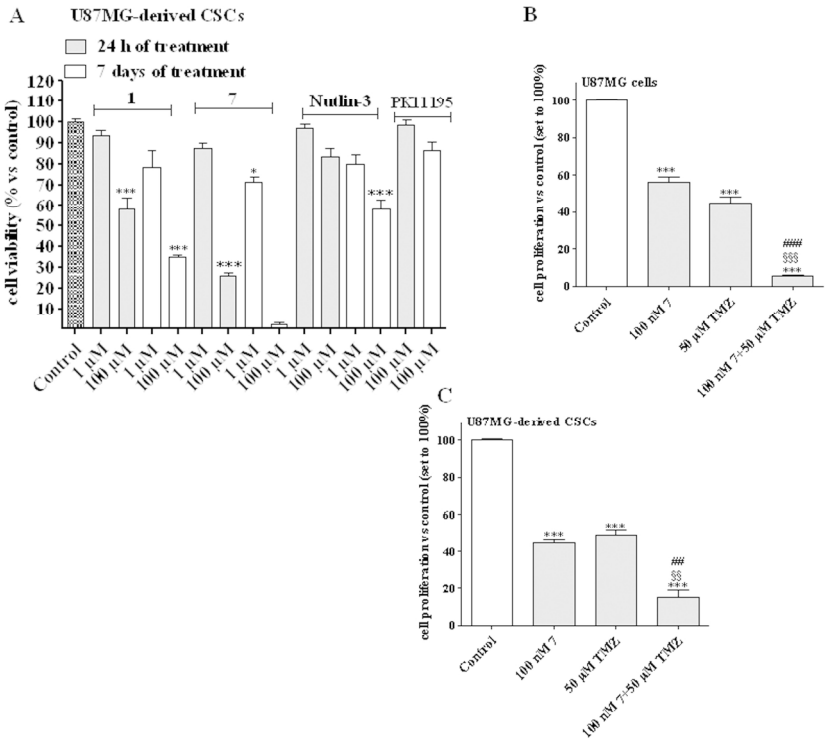

Effects on CSC viability and of TMZ co-treatment. (A) CSCs isolated from U87MG cells were incubated with the indicated concentrations of 1, 7, Nutlin-3 or PK11195 for 24 h or seven days. At the end of treatment, cell viability was measured using MTS assay. The data were expressed as a percentage with respect to that of untreated cells (control), which was set to 100%, and are the mean values ± SEM of three independent experiments, each performed in duplicate. The significance of the differences was determined with a one-way ANOVA with Bonferroni post-test: * P<0.05, *** P<0.001 vs. control. (B, C) U87MG cells (panel B) or U87MG-derived CSCs (panel C) were incubated with 100 nM 7 or 50 μM TMZ for 72 h or seven days, respectively. At the end of treatment, cell viability was measured using MTS assay. The significance of the differences was determined with a one-way ANOVA with Bonferroni post-test: * P<0.05, *** P<0.001 control; ## P<0.01, ### P<0.001 vs. cells treated with 7; §§ P<0.01, §§§ P<0.001 vs. cells treated with TMZ.

190x142mm (300 x 300 DPI)

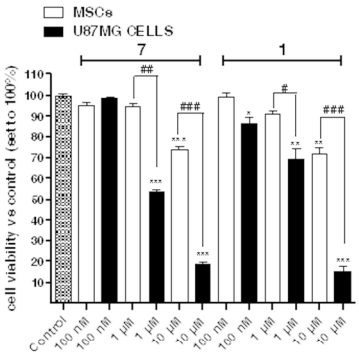

Effects on the viability of normal MSCs. MSCs or U87MG were incubated with the indicated concentration of 1 or 7 for 48 h. At the end of treatment, cell viability was measured using MTS assay. The data were expressed as a percentage with respect to that of untreated cells (control), which was set to 100%, and are the mean values ± SEM of three independent experiments, each performed in duplicate. The significance of the differences was determined with a one-way ANOVA with Bonferroni post-test: * P<0.05, ** P<0.01, *** P<0.001 control; # P<0.05, ## P<0.01, ### P<0.001 vs MSCs.
190x142mm (300 x 300 DPI)